

# A Dual Symmetric Gauss-Seidel Alternating Direction Method of Multipliers for Hyperspectral Sparse Unmixing

Longfei Ren, Chengjing Wang, Peipei Tang, and Zheng Ma, *Member, IEEE*

**Abstract**—Since sparse unmixing has emerged as a promising approach to hyperspectral unmixing, some spatial-contextual information in the hyperspectral images has been exploited to improve the performance of the unmixing recently. The total variation (TV) has been widely used to promote the spatial homogeneity as well as the smoothness between adjacent pixels. However, the computation task for hyperspectral sparse unmixing with a TV regularization term is heavy. Besides, the convergences of the traditional sparse unmixing algorithms which are special cases of the primal alternating direction method of multipliers (pADMM) have not been explained in details. In this paper, we design an efficient and convergent dual symmetric Gauss-Seidel ADMM (sGS-ADMM) for hyperspectral sparse unmixing with a TV regularization term. We also present the global convergence and local linear convergence rate analysis for the traditional sparse unmixing algorithm and our algorithm. As demonstrated in numerical experiments, our algorithm can obviously improve the efficiency of the unmixing compared with the state-of-the-art algorithm. More importantly, we can obtain images with higher quality.

**Index Terms**—Hyperspectral imaging, sparse unmixing, total variation, semi-proximal alternating direction method of multipliers, dual symmetric Gauss-Seidel alternating direction method of multipliers.

## I. INTRODUCTION

IN recent years, the hyperspectral remote sensing technology has been developed significantly. However, the spatial resolution of hyperspectral remote sensing images is low and the mixed pixels are widespread in the observed hyperspectral data. The reason lies in the complexity of the ground surface, the limitation of the spectral acquisition approach as well as the restriction of the hyperspectral imaging instruments. How to extract and separate the pure spectral signatures (endmembers) from the mixed pixels and determine the corresponding proportions (abundances) becomes the key issue for the hyperspectral images analysis and its quantification application.

Hyperspectral unmixing, which decomposes mixed pixels into endmembers and corresponding abundances, has obtained

much attention in recent decades. It has many practical applications in environmental monitoring, mine detection, agricultural industry, and so on. The hyperspectral mixture models can be divided into the linear mixing model (LMM) and nonlinear mixing models (NLMMs) [1]. In the LMM, we assume that the effects of the secondary reflection and multiple scattering have the least influence on the spectral signature. In the NLMMs, we assume that the mixed spectral signature is synthesized by the endmembers according to some nonlinear relationship. For the LMM, each pixel in a hyperspectral image can be linearly decomposed into a number of endmembers weighted by their corresponding abundances. Since the LMM exhibits some practical merits such as its simplicity and ease of implementation, we will focus on the LMM which is also the mainstream of current research on hyperspectral unmixing.

## A. Literature

In the literature, the traditional unmixing based on the LMM includes the geometrical based algorithms and the statistical based algorithms [1]. The geometrical based algorithms generally require the assumption that all the reflection spectrum curves belong to the same geometrical simplex set. The vertices of the simplex set represent the corresponding endmembers. So identifying the endmembers is equivalent to searching for the vertices. The representative algorithms of this class include the vertex component analysis (VCA) algorithm [2], the pixel purity index (PPI) algorithm [3], the simplex growing algorithm (SGA) [4], the minimum volume enclosing simplex (MVES) algorithm [5], the iterative constrained endmembers (ICE) algorithm [6] and the minimum volume transform-nonnegative matrix factorization (MVC-NMF) algorithm [7]. The statistical algorithms, such as the Bayesian techniques, are based on the priori information of the abundances of endmembers [8] for the variability modeling in a natural framework.

With the explosive development of compressive sensing [9]–[11], the sparsity based approaches have recently emerged as a promising alternative for hyperspectral unmixing. The sparsity based approaches aim at finding the optimal subset of a (potentially very large) spectral library in a semisupervised way. The optimal subset is also the best one that can simulate each pixel of a given hyperspectral image. As shown in [12], the sparsity based approaches have attracted many interests as they do not require the presence of pure pixels in a given scene and do not need to estimate the number of endmembers

The work of Peipei Tang was supported by the Natural Science Foundation of Zhejiang Province of China under Grant LY19A010028 and the Science & Technology Development Project of Hangzhou, China under Grant 20170533B22.

L. Ren and Z. Ma are with the Provincial Key Lab of Information Coding and Transmission, Southwest Jiaotong University, Chengdu 610031, China (e-mails: renlf@my.swjtu.edu.cn; zma@home.swjtu.edu.cn).

C. Wang is with School of Mathematics, Southwest Jiaotong University, Chengdu 611756, China (e-mail: renascencewang@hotmail.com).

P. Tang is with School of Computer and Computing Science, Zhejiang University City College, Hangzhou 310015, China (e-mail: tangpp@zucc.edu.cn).

in the data, which are two obstacles of the traditional unmixing methods. In practice, the number of endmembers in the real scene is far less than the number of endmembers in the spectral library. This means that the abundances corresponding to the spectral library are sparse. As a result, the sparsity based approaches are related to the linear sparse regression techniques. The traditional  $l_0$  norm is widely used as a sparse regularization factor. However, the  $l_0$  regularization problem is a nonconvex nonsmooth NP-hard problem. Fortunately, Candès *et al.* [13] proved that the  $l_1$  regularization problem has the same solution as the  $l_0$  regularization under the so called restricted isometric property (RIP). This gives a new perspective to the convex approximation of the  $l_0$  norm with the  $l_1$  norm under certain conditions.

Iordache *et al.* [14] first added the sparsity constraint to the hyperspectral unmixing model and proposed a sparse unmixing by the variable splitting and augmented Lagrangian (SUnSAL) algorithm. This opens a new gate so that the abundance estimation neither depends on the purity of the spectra nor a good endmember extraction algorithm. Subsequently, Iordache *et al.* [15] proposed the sparse unmixing via the variable splitting augmented Lagrangian and total variation (SUnSAL-TV) algorithm to deal with the hyperspectral unmixing model plus a total variation (TV). The TV, which promotes the spatial homogeneity as well as the smoothness between adjacent pixels, has been widely used in image processing [16]–[19]. So the SUnSAL-TV algorithm significantly improves the performance of unmixing. Meanwhile, as shown in [20] and [21], the unmixing performance based on nonisotropic TV is better than that on isotropic TV. From the other point of view, the collaborative sparse unmixing by the variable splitting and augmented Lagrangian (CLSUnSAL) algorithm in [22] takes into account the entire abundances matrix globally. The global row sparsity to all pixels in the hyperspectral images is considered as a constraint. The collaborative SUnSAL-TV (CLSUnSAL-TV) algorithm [23] takes the combination of the spatial correlation and the global row sparsity into consideration. Although the numerical experiments show that the SUnSAL-TV algorithm and the CLSUnSAL-TV algorithm work well, the convergences of the two algorithms have not been guaranteed in theory. Therefore we need to design an efficient and convergent algorithm.

As we all know, all the algorithms we mentioned above are essentially the special cases of the alternating direction method of multipliers (ADMM) applied to the primal problem. So we may call it pADMM. The semi-proximal ADMM (SPADMM) was originally proposed in 1970s. One may see [24] and [25] for details. If the semi-proximal term vanishes, then it is the classical ADMM. We refer the readers to [26] and [27] for a better understanding of the historical development of the classic ADMM. We also refer the readers to [28] and [29] for the global convergence and linear convergence rate of the SPADMM for convex problems. The ADMM can solve a great deal of problems successfully. However the convergence of the ADMM is only guaranteed to those problems with 2 blocks. As for the 3-block (and beyond) problems, the extended version of the ADMM may not converge. One may see a counter example in [30]. Recently in [31], a symmetric

Gauss-Seidel (sGS) method was designed for the multi-block convex problems. But note that this algorithm can only deal with problems with one nonsmooth block.

## B. Contributions

The main contributions of this paper are as follows. Firstly, we design a dual symmetric Gauss-Seidel ADMM (sGS-ADMM) to solve the hyperspectral sparse unmixing with a TV regularization term. Secondly, we present the global convergence and local linear convergence rate of the pADMM and the dual sGS-ADMM. As shown in the numerical experiments, the dual sGS-ADMM is about 10 times faster than the pADMM.

## C. Structure

The remaining parts of this paper are organized as follows. In the next section, we will introduce some basic notations, definitions and the block sGS method. We should mention that the block sGS method plays a pivotal role in our algorithm. In Section III, we will describe the model of hyperspectral unmixing. In Section IV, we will recall the pADMM and present the global convergence and local linear convergence rate of the pADMM. In Section V, we will propose the dual sGS-ADMM. Then we also present the global convergence and local linear convergence rate of the dual sGS-ADMM. Numerical experiments will demonstrate the efficiency of the proposed algorithm in Section VI. The conclusion will be discussed in Section VII.

## II. PRELIMINARIES

In this section, we first introduce some basic notations and definitions in convex analysis. We refer the reader to a bible book of convex analysis [32] for more in-depth contents. Then we introduce an efficient and elegant sGS decomposition which will be used to solve the subproblems of the dual sGS-ADMM.

### A. Notations and definitions

Let  $\mathcal{X}$  be a finite dimensional real Hilbert space. Let  $\mathbf{C}$  be a subset of  $\mathcal{X}$ . The indicator function of  $\mathbf{C}$  is defined by  $\delta_{\mathbf{C}}(\mathbf{x})$ , i.e.,  $\delta_{\mathbf{C}}(\mathbf{x}) = 0$  if  $\mathbf{x} \in \mathbf{C}$  and  $\delta_{\mathbf{C}}(\mathbf{x}) = +\infty$  if  $\mathbf{x} \notin \mathbf{C}$ . For  $\mathbf{X} \in R^{m \times n}$ , the Frobenius norm of  $\mathbf{X}$  is defined by  $\|\mathbf{X}\|_F = \sqrt{\text{trace}(\mathbf{X}\mathbf{X}^T)}$ . The  $l_{1,1}$  and  $l_{2,1}$  norms of  $\mathbf{X}$  are defined by  $\|\mathbf{X}\|_{1,1} := \|\mathbf{X}\|_1 = \sum_{j=1}^n \sum_{i=1}^m |\mathbf{X}_{ij}|$  and  $\|\mathbf{X}\|_{2,1} := \sum_{k=1}^m \|\mathbf{X}^k\|_2$ , respectively, where  $\mathbf{X}^k$  is the  $k$ -th row of  $\mathbf{X}$ . For any given self-adjoint positive semidefinite linear operator  $\mathcal{M} : \mathcal{X} \rightarrow \mathcal{X}$ ,  $\text{dist}_{\mathcal{M}}(\mathbf{x}, \mathbf{S}) := \inf_{\mathbf{x}' \in \mathbf{S}} \|\mathbf{x} - \mathbf{x}'\|_{\mathcal{M}}$  for all  $\mathbf{x} \in \mathcal{X}$  and  $\mathbf{S} \in \mathcal{X}$ , where  $\|\mathbf{x}\|_{\mathcal{M}} := \sqrt{\langle \mathbf{x}, \mathcal{M}\mathbf{x} \rangle}$ . The symbols  $\mathcal{I}$ ,  $\mathbf{1}$ ,  $\mathbf{0}$  denote the identity mapping, the all-ones matrix and the all-zeros matrix, respectively.

*Definition 1* [32, Section 12]: Let  $p : R^n \rightarrow R$ . The conjugate function of  $p$  is defined as

$$p^*(\mathbf{y}) := \sup_{\mathbf{x} \in \text{dom}(p)} \{\mathbf{y}^T \mathbf{x} - p(\mathbf{x})\},$$

where  $\text{dom}(p) := \{\mathbf{x} \in R^n \mid p(\mathbf{x}) < +\infty\}$ .

**Definition 2** [34, Definition 2.2.1]: A set which can be expressed as the intersection of finitely many closed half spaces of  $R^n$  is called a convex polyhedron. A polyhedral set is the union of finitely many convex polyhedrals. A function is called piecewise quadratic (linear) if its domain is a polyhedral set and it is quadratic (affine) on each of the convex polyhedral which constitutes its domain.

**Definition 3** [32, Section 31]: For a given closed proper convex function  $p : \mathcal{X} \rightarrow (-\infty, +\infty]$ , the proximal mapping  $\text{Prox}_p(\cdot)$  associated with  $p$  is defined by

$$\text{Prox}_p(\mathbf{x}) := \underset{\mathbf{u}}{\text{argmin}} \left\{ p(\mathbf{u}) + \frac{1}{2} \|\mathbf{u} - \mathbf{x}\|_2^2 \right\}, \forall \mathbf{x} \in \mathcal{X}.$$

**Definition 4** [32, Section 24]: Let  $\mathbf{H}$  be a real Hilbert space with an inner product  $\langle \cdot, \cdot \rangle$ . A multifunction  $F : \mathbf{H} \rightrightarrows \mathbf{H}$  is said to be a monotone operator if

$$\langle \mathbf{z} - \mathbf{z}', \mathbf{w} - \mathbf{w}' \rangle \geq 0, \quad \forall \mathbf{w} \in F(\mathbf{z}), \mathbf{w}' \in F(\mathbf{z}').$$

It is said to be maximal monotone if, in addition, the graph

$$\text{gph}(F) := \{(\mathbf{z}, \mathbf{w}) \in \mathbf{H} \times \mathbf{H} \mid \mathbf{w} \in F(\mathbf{z})\}$$

is not properly contained in the graph of any other monotone operator  $F' : \mathbf{H} \rightrightarrows \mathbf{H}$ .

**Definition 5** [36, Section 3.8]: Let  $(\mathbf{x}^0, \mathbf{y}^0) \in \text{gph}(F)$ . The multi-valued mapping  $F : \mathcal{X} \rightrightarrows \mathcal{Y}$  is said to be calm at  $\mathbf{x}^0$  for  $\mathbf{y}^0$  with modulus  $\kappa_0 \geq 0$  if there exist a neighborhood  $V$  of  $\mathbf{x}^0$  and a neighborhood  $W$  of  $\mathbf{y}^0$  such that

$$F(\mathbf{x}) \cap W \subseteq F(\mathbf{x}^0) + \kappa_0 \|\mathbf{x} - \mathbf{x}^0\| B_{\mathbf{y}}, \quad \forall \mathbf{x} \in V,$$

where  $B_{\mathbf{y}}$  is the unit ball in  $\mathcal{Y}$ .

### B. An inexact block sGS method

In this subsection, we briefly introduce some preliminaries of an inexact sGS method. For more details, one may refer to [31].

Let  $\mathcal{X} := \mathcal{X}_1 \times \mathcal{X}_2 \times \cdots \times \mathcal{X}_s$  with  $\mathcal{X}_i$  being finite dimensional real Euclidean spaces, where  $s \geq 2$  is a given integer. For any  $\mathbf{x} \in \mathcal{X}$ , we denote  $\mathbf{x} = (\mathbf{x}_1, \mathbf{x}_2, \dots, \mathbf{x}_s)$  with  $\mathbf{x}_i \in \mathcal{X}_i$ ,  $i = 1, \dots, s$ . Let  $\mathcal{Q} : \mathcal{X} \rightarrow \mathcal{X}$  be a given self-adjoint positive semidefinite linear operator defined by

$$\mathcal{Q}\mathbf{x} := \begin{pmatrix} \mathcal{Q}_{1,1} & \mathcal{Q}_{1,2} & \cdots & \mathcal{Q}_{1,s} \\ \mathcal{Q}_{1,2}^* & \mathcal{Q}_{2,2} & \cdots & \mathcal{Q}_{2,s} \\ \vdots & \vdots & \ddots & \vdots \\ \mathcal{Q}_{1,s}^* & \mathcal{Q}_{2,s}^* & \cdots & \mathcal{Q}_{s,s} \end{pmatrix} \begin{pmatrix} \mathbf{x}_1 \\ \mathbf{x}_2 \\ \vdots \\ \mathbf{x}_s \end{pmatrix},$$

where  $\mathcal{Q}_{i,i} : \mathcal{X}_i \rightarrow \mathcal{X}_i$  ( $i = 1, \dots, s$ ) are self-adjoint positive definite linear operators,  $\mathcal{Q}_{i,j} : \mathcal{X}_j \rightarrow \mathcal{X}_i$  ( $i = 1, \dots, s-1, j > i$ ) are linear operators and  $\mathcal{Q}_{i,j}^* : \mathcal{X}_i \rightarrow \mathcal{X}_j$  are the adjoints of  $\mathcal{Q}_{i,j}$ . Let  $\mathbf{r} = (\mathbf{r}_1, \mathbf{r}_2, \dots, \mathbf{r}_s) \in \mathcal{X}$  be given. Define  $h : \mathcal{X} \rightarrow R$  by

$$h(\mathbf{x}) := \frac{1}{2} \langle \mathbf{x}, \mathcal{Q}\mathbf{x} \rangle - \langle \mathbf{r}, \mathbf{x} \rangle, \quad \mathbf{x} \in \mathcal{X}.$$

Let  $\phi : \mathcal{X}_1 \rightarrow (-\infty, +\infty]$  be a given lower semi-continuous proper convex function. Define a self-adjoint positive semidefinite linear operator  $\mathcal{T} : \mathcal{X} \rightarrow \mathcal{X}$  by

$$\mathcal{T} = \mathcal{U}\mathcal{D}^{-1}\mathcal{U}^*,$$

where

$$\mathcal{U} := \begin{pmatrix} 0 & \mathcal{Q}_{1,2} & \cdots & \mathcal{Q}_{1,s} \\ 0 & 0 & \cdots & \mathcal{Q}_{2,s} \\ \vdots & \vdots & \ddots & \vdots \\ 0 & 0 & \cdots & 0 \end{pmatrix}$$

and

$$\mathcal{D} := \text{Diag}(\mathcal{Q}_{1,1}, \dots, \mathcal{Q}_{s,s}).$$

Suppose that  $\hat{\delta}_i$  and  $\delta_i$  are given error tolerance vectors in  $\mathcal{X}_i$  with  $\hat{\delta}_1 = \delta_1$ . Denote  $\hat{\delta} = (\hat{\delta}_1, \dots, \hat{\delta}_s)$ ,  $\delta = (\delta_1, \dots, \delta_s)$ , and

$$\Delta(\hat{\delta}, \delta) := \delta + \mathcal{U}\mathcal{D}^{-1}(\delta - \hat{\delta}).$$

Define  $\mathbf{x}_{\leq i} := (\mathbf{x}_1, \mathbf{x}_2, \dots, \mathbf{x}_i)$ ,  $\mathbf{x}_{\geq i} := (\mathbf{x}_i, \mathbf{x}_{i+1}, \dots, \mathbf{x}_s)$ ,  $i = 0, 1, \dots, s+1$  with the convention that  $\mathbf{x}_{\leq 0} = \mathbf{x}_{\geq s+1} = \emptyset$ . Let  $\bar{\mathbf{x}} \in \mathcal{X}$  be given. Define  $\mathbf{x}^+ \in \mathcal{X}$  by

$$\mathbf{x}^+ = \underset{\mathbf{x}}{\text{argmin}} \left\{ \phi(\mathbf{x}_1) + h(\mathbf{x}) + \frac{1}{2} \|\mathbf{x} - \bar{\mathbf{x}}\|_{\mathcal{T}}^2 - \langle \Delta(\hat{\delta}, \delta), \mathbf{x} \rangle \right\}. \quad (1)$$

If  $\delta = \hat{\delta} = 0$ , it means that the problem (1) can be solved exactly without any error.

The following sGS decomposition was introduced by Li, Sun and Toh [31] which is a core technique to design our algorithm.

**Proposition 1:** [31, Theorem 1] Assume that the self-adjoint linear operators  $\mathcal{Q}_{i,i}$  are positive definite for  $i = 1, 2, \dots, s$ . Then we have

$$\mathcal{Q} + \mathcal{T} = (\mathcal{D} + \mathcal{U})\mathcal{D}^{-1}(\mathcal{D} + \mathcal{U}^*).$$

For  $i = s, \dots, 2$ , suppose that we have computed  $\hat{\mathbf{x}}_i \in \mathcal{X}_i$  which are defined as follows:

$$\begin{aligned} \hat{\mathbf{x}}_i &= \underset{\mathbf{x}_i}{\text{argmin}} \left\{ \phi(\bar{\mathbf{x}}_1) + h(\bar{\mathbf{x}}_{\leq i-1}, \mathbf{x}_i, \hat{\mathbf{x}}_{\geq i+1}) - \langle \hat{\delta}_i, \mathbf{x}_i \rangle \right\} \\ &= \mathcal{Q}_{i,i}^{-1} \left( \mathbf{r}_i + \hat{\delta}_i - \sum_{j=1}^{i-1} \mathcal{Q}_{i,j}^* \bar{\mathbf{x}}_j - \sum_{j=i+1}^s \mathcal{Q}_{i,j} \hat{\mathbf{x}}_j \right). \end{aligned}$$

Then the optimal solution  $\mathbf{x}^+$  defined by (1) can be obtained exactly via

$$\begin{cases} \mathbf{x}_1^+ &= \underset{\mathbf{x}_1}{\text{argmin}} \left\{ \phi(\mathbf{x}_1) + h(\mathbf{x}_1, \hat{\mathbf{x}}_{\geq 2}) - \langle \delta_1, \mathbf{x}_1 \rangle \right\}, \\ \mathbf{x}_i^+ &= \underset{\mathbf{x}_i}{\text{argmin}} \left\{ \phi(\mathbf{x}_1^+) + h(\mathbf{x}_{\leq i-1}^+, \mathbf{x}_i, \hat{\mathbf{x}}_{\geq i+1}) - \langle \delta_i, \mathbf{x}_i \rangle \right\}, \\ &= \mathcal{Q}_{i,i}^{-1} \left( \mathbf{r}_i + \delta_i - \sum_{j=1}^{i-1} \mathcal{Q}_{j,i}^* \mathbf{x}_j^+ - \sum_{j=i+1}^s \mathcal{Q}_{i,j} \hat{\mathbf{x}}_j \right), \\ &\quad i = 2, \dots, s. \end{cases}$$

We can see from above that solving a cycle of optimization problems in Proposition 1 is equivalent to solving the problem (1).

### III. SYSTEM MODEL

For the LMM, we assume that the spectrum of each mixed pixels can be represented as a linear combination of each endmember spectrum in any given spectral band (see [1]). That is, for each mixed pixels, the linear model can be written as

$$\mathbf{y} = \mathbf{M}\mathbf{s} + \mathbf{n},$$

where  $\mathbf{y} := [\mathbf{y}_1, \mathbf{y}_2, \dots, \mathbf{y}_L]^T$  denotes the measured spectra of the mixed pixels and  $L$  denotes the number of bands,  $\mathbf{M} := [\mathbf{m}_1, \mathbf{m}_2, \dots, \mathbf{m}_q]$  denotes the endmembers matrix,  $q$  denotes the number of endmembers and each  $\mathbf{m}_j := [\mathbf{m}_{1j}, \mathbf{m}_{2j}, \dots, \mathbf{m}_{Lj}]^T$  denotes the spectra signature of the  $j$ -th endmembers,  $\mathbf{s} := [\mathbf{s}_1, \mathbf{s}_2, \dots, \mathbf{s}_q]^T$  denotes the abundances of the endmembers and  $\mathbf{n} := [\mathbf{n}_1, \mathbf{n}_2, \dots, \mathbf{n}_L]^T$  denotes the error vector. According to the physical meaning of the real scene, the abundances need to satisfy the so called abundance non-negativity constraint (ANC) and the abundance sum constraint (ASC) [1]. That is,

$$\begin{aligned} \mathbf{s}_i &\geq 0, \quad \forall i = 1, 2, \dots, q, \\ \sum_{i=1}^q \mathbf{s}_i &= 1. \end{aligned}$$

As mentioned previously, the sparsity based approaches proposed by Iordache *et al.* [1] replace the endmembers matrix  $\mathbf{M}$  by a known spectral library  $\mathbf{A} \in R^{L \times m}$  [14]. Unmixing then amounts to finding the optimal subset of signatures in  $\mathbf{A}$ . Specially, we have

$$\mathbf{y} = \mathbf{A}\mathbf{x} + \mathbf{n},$$

where  $\mathbf{x} \in R^{m \times 1}$  denotes the abundances corresponding to the library  $\mathbf{A}$ .

As shown in [38], the conventional hyperspectral sparse unmixing can be uniformly expressed as the following model:

$$\begin{aligned} \min_{\mathbf{X}} \quad & \frac{1}{2} \|\mathbf{A}\mathbf{X} - \mathbf{Y}\|_F^2 + \lambda \|\mathbf{X}\|_{\rho,1} + \lambda_{TV} TV(\mathbf{X}) \\ \text{s.t.} \quad & \mathbf{X} \geq 0, \end{aligned} \quad (2)$$

where

$$TV(\mathbf{X}) := \sum_{\{i,j\} \in \varepsilon} \|\mathbf{x}_i - \mathbf{x}_j\|_1$$

is a vector extension of the nonisotropic  $TV$ ,  $\varepsilon$  denotes the set of horizontal and vertical neighbors of  $\mathbf{X}$ ,  $\lambda, \lambda_{TV} \geq 0$  are given parameters,  $\mathbf{Y} = [\mathbf{y}_1, \mathbf{y}_2, \dots, \mathbf{y}_n] \in R^{L \times n}$  denotes the observed data,  $\mathbf{X} = [\mathbf{x}_1, \mathbf{x}_2, \dots, \mathbf{x}_n] \in R^{m \times n}$  denotes the abundances matrix and  $n$  denotes the number of the pixels. When  $\rho = 1, \lambda_{TV} = 0$ , (2) is reduced to the sparse unmixing (SUn) model. When  $\rho = 2, \lambda_{TV} = 0$ , (2) is actually the collaborative sparse unmixing (CLSUn) model. Similarly, we refer to (2) with  $\rho = 1$  as the sparse unmixing with TV (SUnTV) model and  $\rho = 2$  as the collaborative sparse unmixing with TV (CLSUnTV) model.

For the design of the algorithm, we need to give a more detailed characterization of the TV norm.

Suppose  $n = n_r \times n_c$ , where  $n_r$  and  $n_c$  denote the dimensions of the rows and columns of the pixels, respectively. Let

$$\mathbf{X} := [\mathbf{x}_1, \mathbf{x}_2, \dots, \mathbf{x}_{n_r}, \mathbf{x}_{n_r+1}, \mathbf{x}_{n_r+2}, \dots, \mathbf{x}_{2n_r}, \dots, \mathbf{x}_{n-n_r+1}, \mathbf{x}_{n-n_r+2}, \dots, \mathbf{x}_n],$$

$$\mathbf{X}' := \begin{pmatrix} \mathbf{x}_1 & \mathbf{x}_{n_r+1} & \cdots & \mathbf{x}_{n-n_r+1} \\ \mathbf{x}_2 & \mathbf{x}_{n_r+2} & \cdots & \mathbf{x}_{n-n_r+2} \\ \vdots & \vdots & \ddots & \vdots \\ \mathbf{x}_{n_r} & \mathbf{x}_{2n_r} & \cdots & \mathbf{x}_n \end{pmatrix} \in R^{(m \times n_r) \times n_c},$$

$$\mathbf{X}'' := \begin{pmatrix} \mathbf{x}_1 & \mathbf{x}_2 & \cdots & \mathbf{x}_{n_r} \\ \mathbf{x}_{n_r+1} & \mathbf{x}_{n_r+2} & \cdots & \mathbf{x}_{2n_r} \\ \vdots & \vdots & \ddots & \vdots \\ \mathbf{x}_{n-n_r+1} & \mathbf{x}_{n-n_r+2} & \cdots & \mathbf{x}_n \end{pmatrix} \in R^{(m \times n_c) \times n_r},$$

Define two linear operators  $\mathcal{B} : R^{(m \times n_r) \times n_c} \rightarrow R^{(m \times n_r) \times (n_c-1)}$  and  $\mathcal{C} : R^{(m \times n_c) \times n_r} \rightarrow R^{(m \times n_c) \times (n_r-1)}$  to compute the horizontal differences between the neighboring pixels of  $\mathbf{X}'$  and  $\mathbf{X}''$ .

$$\mathcal{B}\mathbf{X}' := \begin{pmatrix} c_1 & c_{n_r+1} & \cdots & c_{n-2n_r+1} \\ c_2 & c_{n_r+2} & \cdots & c_{n-2n_r+2} \\ \vdots & \vdots & \ddots & \vdots \\ c_{n_r} & c_{2n_r} & \cdots & c_{n-n_r} \end{pmatrix},$$

$$\mathcal{C}\mathbf{X}'' := \begin{pmatrix} e_1 & e_2 & \cdots & e_{n_r-1} \\ e_{n_r+1} & e_{n_r+2} & \cdots & e_{2n_r-1} \\ \vdots & \vdots & \ddots & \vdots \\ e_{n-n_r+1} & e_{n-n_r+2} & \cdots & e_{n-1} \end{pmatrix},$$

where  $\mathbf{c}_i = \mathbf{x}_{i+n_r} - \mathbf{x}_i$  ( $i = 1, \dots, n-n_r$ ) and  $\mathbf{e}_i = \mathbf{x}_{i+1} - \mathbf{x}_i$  ( $i = 1, \dots, n_r-1, n_r+1, \dots, 2n_r-1, \dots, n-n_r+1, \dots, n-1$ ). Define two linear operators  $\hat{\mathcal{H}}_v : R^{m \times n} \rightarrow R^{m \times (n-n_r)}$  and  $\hat{\mathcal{H}}_h : R^{m \times n} \rightarrow R^{m \times (n-n_c)}$ :

$$\begin{aligned} \hat{\mathcal{H}}_v \mathbf{X} &= [\mathbf{c}_1, \mathbf{c}_2, \dots, \mathbf{c}_{n-n_r}], \\ \hat{\mathcal{H}}_h \mathbf{X} &= [\mathbf{e}_1, \dots, \mathbf{e}_{n_r-1}, \mathbf{e}_{n_r+1}, \dots, \mathbf{e}_{2n_r-1}, \\ &\quad \dots, \mathbf{e}_{n-n_r+1}, \dots, \mathbf{e}_{n-1}]. \end{aligned}$$

Then the problem (2) can be reformulated to

$$\begin{aligned} \min_{\mathbf{X}} \quad & \frac{1}{2} \|\mathbf{A}\mathbf{X} - \mathbf{Y}\|_F^2 + \lambda \|\mathbf{X}\|_{\rho,1} + \lambda_{TV} \|\hat{\mathcal{H}}_v \mathbf{X}\|_1 + \\ & \lambda_{TV} \|\hat{\mathcal{H}}_h \mathbf{X}\|_1 + \delta_{R_+^{m \times n}}(\mathbf{X}). \end{aligned} \quad (3)$$

We should mention that there is a slight difference between the way we handle the TV norm with that in [15]. In our framework, we assume that the rightmost (lowest) boundaries have no right (lower) neighboring pixels. Actually it is more reasonable. Instead, in [15], they assume periodic boundaries. In order to be consistent, we keep the way in [15] when using the pADMM. In [15], they define two linear operators  $\mathcal{H}_h : R^{m \times n} \rightarrow R^{m \times n}$  and  $\mathcal{H}_v : R^{m \times n} \rightarrow R^{m \times n}$  to compute the horizontal and vertical differences between the neighboring pixels of  $\mathbf{X}$  as follows

$$\mathcal{H}_h \mathbf{X} = [\mathbf{d}_1, \mathbf{d}_2, \dots, \mathbf{d}_n],$$

$$\mathcal{H}_v \mathbf{X} = [\mathbf{b}_1, \mathbf{b}_2, \dots, \mathbf{b}_n],$$

where  $\mathbf{d}_i = \mathbf{x}_i - \mathbf{x}_{i_h}$  and  $\mathbf{b}_i = \mathbf{x}_i - \mathbf{x}_{i_v}$  ( $i = 1, \dots, n$ ), with  $i$  denoting an index of a pixel,  $i_h$  and  $i_v$  denoting the indices of the corresponding horizontal and vertical neighbors. Let

$$\mathcal{H}\mathbf{X} = \begin{bmatrix} \mathcal{H}_h \mathbf{X} \\ \mathcal{H}_v \mathbf{X} \end{bmatrix}.$$

An equivalent form of the problem (2) is

$$\begin{aligned} \min_{\mathbf{X}} \quad & \frac{1}{2} \|\mathbf{A}\mathbf{X} - \mathbf{Y}\|_F^2 + \lambda \|\mathbf{X}\|_{\rho,1} + \lambda_{TV} \|\mathcal{H}\mathbf{X}\|_1 \\ \text{s.t.} \quad & \mathbf{X} \geq 0. \end{aligned} \quad (4)$$

#### IV. THE PADMM

In this section we first recall the SUnSAL-TV algorithm and the CLSUnSAL-TV algorithm, both of which are essentially the pADMM. Then we present the global convergence and local linear convergence rate of the pADMM.

##### A. The pADMM

We can reformulate (4) equivalently by introducing some slack variables

$$\begin{aligned} \min_{\tilde{\mathbf{D}}, \mathbf{D}_1, \mathbf{D}_2, \mathbf{D}_3, \mathbf{D}_4, \mathbf{D}_5} \quad & \frac{1}{2} \|\mathbf{D}_1 - \mathbf{Y}\|_F^2 + \lambda \|\mathbf{D}_2\|_{\rho,1} + \lambda_{TV} \|\mathbf{D}_4\|_1 \\ & + \delta_{R_+^{m \times n}}(\mathbf{D}_5) \\ \text{s.t.} \quad & \mathbf{D}_1 = \mathbf{A}\tilde{\mathbf{D}}, \mathbf{D}_2 = \tilde{\mathbf{D}}, \mathbf{D}_3 = \tilde{\mathbf{D}}, \\ & \mathbf{D}_4 = \mathcal{H}\mathbf{D}_3, \mathbf{D}_5 = \tilde{\mathbf{D}}, \end{aligned} \quad (5)$$

where  $\tilde{\mathbf{D}} \in R^{m \times n}$ ,  $\mathbf{D}_1 \in R^{L \times n}$ ,  $\mathbf{D}_2 \in R^{m \times n}$ ,  $\mathbf{D}_3 \in R^{m \times n}$ ,  $\mathbf{D}_4 \in R^{2m \times n}$ ,  $\mathbf{D}_5 \in R^{m \times n}$ .

The above problem can also be written in the following form

$$\begin{aligned} \min_{\mathbf{M}, \mathbf{N}} \quad & f(\mathbf{M}) + g(\mathbf{N}) \\ \text{s.t.} \quad & \mathbf{F}\mathbf{M} + \mathbf{G}\mathbf{N} = \mathbf{0}, \end{aligned} \quad (6)$$

where

$$\begin{aligned} \mathbf{M} &= (\tilde{\mathbf{D}}^T, \mathbf{D}_1^T, \mathbf{D}_2^T, \mathbf{D}_3^T)^T \in R^{(3m+L) \times n}, \\ \mathbf{N} &= (\mathbf{D}_4^T, \mathbf{D}_5^T)^T \in R^{3m \times n}, \\ f(\mathbf{M}) &= \frac{1}{2} \|\mathbf{D}_1 - \mathbf{Y}\|_F^2 + \lambda \|\mathbf{D}_2\|_{\rho,1}, \\ g(\mathbf{N}) &= \lambda_{TV} \|\mathbf{D}_4\|_1 + \delta_{R_+^{m \times n}}(\mathbf{D}_5), \\ \mathbf{F} &= \begin{pmatrix} \mathbf{A} & -\mathbf{I}_{L \times L} & \mathbf{0}_{L \times m} & \mathbf{0}_{L \times m} \\ \mathbf{I}_{m \times m} & \mathbf{0}_{m \times L} & -\mathbf{I}_{m \times m} & \mathbf{0}_{m \times m} \\ \mathbf{I}_{m \times m} & \mathbf{0}_{m \times L} & \mathbf{0}_{m \times m} & -\mathbf{I}_{m \times m} \\ \mathbf{0}_{2m \times m} & \mathbf{0}_{2m \times L} & \mathbf{0}_{2m \times m} & \mathcal{H} \\ \mathbf{I}_{m \times m} & \mathbf{0}_{m \times L} & \mathbf{0}_{m \times m} & \mathbf{0}_{m \times m} \end{pmatrix}, \\ \mathbf{G} &= \begin{pmatrix} \mathbf{0}_{L \times 2m} & \mathbf{0}_{L \times m} \\ \mathbf{0}_{m \times 2m} & \mathbf{0}_{m \times m} \\ \mathbf{0}_{m \times 2m} & \mathbf{0}_{m \times m} \\ -\mathbf{I}_{2m \times 2m} & \mathbf{0}_{2m \times m} \\ \mathbf{0}_{m \times 2m} & -\mathbf{I}_{m \times m} \end{pmatrix}. \end{aligned}$$

Let  $\sigma > 0$  be a given positive number.  $\mathbf{\Lambda} := (\mathbf{\Lambda}_1^T, \mathbf{\Lambda}_2^T, \mathbf{\Lambda}_3^T, \mathbf{\Lambda}_4^T, \mathbf{\Lambda}_5^T)^T \in R^{(5m+L) \times n}$  denotes the Lagrange multipliers of the constraints. The augmented Lagrangian function for the problem (6) is

$$\begin{aligned} L_\sigma(\mathbf{M}, \mathbf{N}; \mathbf{\Lambda}) &= f(\mathbf{M}) + g(\mathbf{N}) + \frac{\sigma}{2} \|\mathbf{F}\mathbf{M} + \mathbf{G}\mathbf{N} - \sigma^{-1} \mathbf{\Lambda}\|_F^2 \\ &\quad - \frac{1}{2\sigma} \|\mathbf{\Lambda}\|_F^2. \end{aligned} \quad (7)$$

The reader may refer to [15] for a better understanding of the details of Algorithm 1.<sup>1</sup>

<sup>1</sup>We have to emphasize that in [15] the authors deal with the problem (8) in three blocks instead of two blocks when they applied the pADMM. In fact, the problem can be regarded as two blocks. So Algorithm 1 in this paper is a little different with Algorithm 1 in [15]. It not only is faster but also has mathematically guaranteed convergence theory. Actually the code for the algorithm in [15] is in accordance with our two-block pADMM.

---

##### Algorithm 1 The pADMM

---

**Require:** Select an initial point  $(\mathbf{M}^0, \mathbf{N}^0; \mathbf{\Lambda}^0)$ . Set  $k = 0$ , choose  $\sigma > 0$ . Iterate the following steps:

**Step 1.** Compute:

$$\begin{aligned} \mathbf{M}^{k+1} &= \underset{\mathbf{M}}{\operatorname{argmin}} L_\sigma(\mathbf{M}, \mathbf{N}^k; \mathbf{\Lambda}^k), \\ \mathbf{N}^{k+1} &= \underset{\mathbf{N}}{\operatorname{argmin}} L_\sigma(\mathbf{M}^{k+1}, \mathbf{N}; \mathbf{\Lambda}^k). \end{aligned}$$

**Step 2.** Update:

$$\mathbf{\Lambda}^{k+1} = \mathbf{\Lambda}^k - \sigma(\mathbf{F}\mathbf{M}^{k+1} + \mathbf{G}\mathbf{N}^{k+1}).$$


---

##### B. Convergence analysis

In this subsection, we discuss the global convergence and the local linear convergence rate of the pADMM.

Suppose that  $(\mathbf{M}, \mathbf{N}) \in R^{(3m+L) \times n} \times R^{3m \times n}$  is an optimal solution to the problem (6). If there exists  $\mathbf{\Lambda} \in R^{(5m+L) \times n}$  such that  $(\mathbf{M}, \mathbf{N}, \mathbf{\Lambda})$  satisfies the following KKT system

$$\begin{cases} 0 \in \partial f(\mathbf{M}) - \mathbf{F}^T \mathbf{\Lambda}, \\ 0 \in \partial g(\mathbf{N}) - \mathbf{G}^T \mathbf{\Lambda}, \\ \mathbf{F}\mathbf{M} + \mathbf{G}\mathbf{N} = \mathbf{0}, \end{cases} \quad (8)$$

then  $(\mathbf{M}, \mathbf{N}, \mathbf{\Lambda})$  is a KKT point for the problem (6), where  $\partial f$  and  $\partial g$  are the subdifferential mappings of  $f$  and  $g$ . Let  $\Omega$  be the solution set of the KKT system (8). Let  $\mathcal{B}: R^{(5m+L) \times n} \rightarrow R^{(3m+L) \times n} \times R^{3m \times n}$  be a linear operator such that its adjoint  $\mathcal{B}^*(\mathbf{M}, \mathbf{N}) = \mathbf{F}\mathbf{M} + \mathbf{G}\mathbf{N}$ . For any  $\mathbf{u} := (\mathbf{M}, \mathbf{N}, \mathbf{\Lambda})$ , the KKT mapping is defined by

$$\mathbf{Q}(\mathbf{u}) := \begin{pmatrix} \mathbf{M} - \operatorname{Prox}_f(\mathbf{M} + \mathbf{F}^T \mathbf{\Lambda}) \\ \mathbf{N} - \operatorname{Prox}_g(\mathbf{N} + \mathbf{G}^T \mathbf{\Lambda}) \\ \mathbf{F}\mathbf{M} + \mathbf{G}\mathbf{N} \end{pmatrix}.$$

Since the subdifferential mappings of the proper closed convex function  $f$  and  $g$  are maximally monotone [37, Theorem 12.17], there exist two self-adjoint and positive semidefinite linear operators  $\Sigma_f$  and  $\Sigma_g$  such that for all  $\mathbf{s}, \mathbf{s}' \in \operatorname{dom}(f)$ ,  $\varsigma \in \partial f(\mathbf{s})$  and  $\varsigma' \in \partial f(\mathbf{s}')$

$$f(\mathbf{s}) \geq f(\mathbf{s}') + \langle \varsigma', \mathbf{s} - \mathbf{s}' \rangle + \frac{1}{2} \|\mathbf{s} - \mathbf{s}'\|_{\Sigma_f}^2,$$

$$\langle \varsigma - \varsigma', \mathbf{s} - \mathbf{s}' \rangle \geq \|\mathbf{s} - \mathbf{s}'\|_{\Sigma_f}^2,$$

and for all  $\mathbf{t}, \mathbf{t}' \in \operatorname{dom}(g)$ ,  $v \in \partial g(\mathbf{t})$  and  $v' \in \partial g(\mathbf{t}')$

$$g(\mathbf{t}) \geq g(\mathbf{t}') + \langle v', \mathbf{t} - \mathbf{t}' \rangle + \frac{1}{2} \|\mathbf{t} - \mathbf{t}'\|_{\Sigma_g}^2,$$

$$\langle v - v', \mathbf{t} - \mathbf{t}' \rangle \geq \|\mathbf{t} - \mathbf{t}'\|_{\Sigma_g}^2.$$

For the convergence of the pADMM, we need the following constraint qualification.

*Assumption 1:* The KKT system (8) has a non-empty solution set.

Now we present the following global convergence and linear convergence rate of the pADMM. It is a special case of the result derived by the combination of [28, Theorem B.1] and [29, Theorem 2].

*Theorem 1:* Suppose that Assumption 1 holds and  $\mathbf{S} := (1 + \sigma)^{-1} \mathbf{A}^T \mathbf{A} + 2\mathbf{I} - (\mathcal{H}^T \mathcal{H} + \mathbf{I})^{-1}$  is positive definite.

Then there exists a KKT point  $\bar{\mathbf{u}} := (\bar{\mathbf{M}}, \bar{\mathbf{N}}, \bar{\mathbf{A}}) \in \Omega$  such that the sequence  $\{(\mathbf{M}^k, \mathbf{N}^k, \mathbf{A}^k)\}$  generated by Algorithm 1 converges to  $\bar{\mathbf{u}}$ . Assume that  $\mathbf{Q}^{-1}$  is calm at the origin for  $\bar{\mathbf{u}}$  with modulus  $\eta > 0$ , i.e., there exists  $r > 0$  such that

$$\text{dist}(\mathbf{u}, \Omega) \leq \eta \|\mathbf{Q}(\mathbf{u})\|, \quad \forall \mathbf{u} \in \{\mathbf{u} : \|\mathbf{u} - \bar{\mathbf{u}}\| \leq r\}.$$

Then there exists an integer  $\bar{k} \geq 1$  such that for all  $k \geq \bar{k}$ ,

$$\text{dist}_{\mathcal{M}}^2(\mathbf{u}^{k+1}, \Omega) \leq \mu \text{dist}_{\mathcal{M}}^2(\mathbf{u}^k, \Omega),$$

where  $\mu \in (0, 1)$  and

$$\mathcal{M} := \text{Diag}(\Sigma_f, \Sigma_g + \sigma \mathcal{I}, (\tau\sigma)^{-1} \mathcal{I}) + \frac{\sigma}{4} \mathcal{B} \mathcal{B}^*,$$

Moreover, there exists a positive number  $\varsigma \in [\mu, 1)$  such that for all  $k \geq 1$

$$\text{dist}_{\mathcal{M}}^2(\mathbf{u}^{k+1}, \Omega) \leq \varsigma \text{dist}_{\mathcal{M}}^2(\mathbf{u}^k, \Omega).$$

*Proof:* See Appendix A.  $\square$

*Remark 1:* Theorem 1 just gives a general result on the linear rate of convergence for Algorithm 1. It is obvious that the core assumption of Theorem 1 is the calmness condition, which is often too strict. For the case of  $\rho = 1$  in the problem (2),  $f$  and  $g$  are piecewise linear-quadratic functions. From [34, Proposition 2.24], we know that  $\mathbf{Q}^{-1}$  is piecewise polyhedral, and furthermore the calmness condition holds automatically by [35, Corollary].

## V. A DUAL SGS-ADMM

In this section, we first propose an sGS-ADMM for the problem (3), then we present the global convergence and local linear convergence rate of the algorithm.

### A. A dual sGS-ADMM

Now we introduce a more efficient dual sGS-ADMM to solve the problem (3).

Let

$$\begin{aligned} p(\mathbf{X}) &= \lambda \|\mathbf{X}\|_{\rho,1} + \lambda_{TV} \|\hat{\mathcal{H}}_v \mathbf{X}\|_1 + \delta_{R_+^{m \times n}}(\mathbf{X}), \\ q(\mathbf{X}) &= \lambda_{TV} \|\hat{\mathcal{H}}_h \mathbf{X}\|_1. \end{aligned}$$

Then the problem (3) can be written in a simple form as below

$$\min_{\mathbf{X}} \frac{1}{2} \|\mathbf{A}\mathbf{X} - \mathbf{Y}\|_F^2 + p(\mathbf{X}) + q(\mathbf{X}). \quad (9)$$

By introducing three slack variables  $\mathbf{U}_1$ ,  $\mathbf{U}_2$  and  $\mathbf{U}_3$ , (9) can be written as

$$\begin{aligned} \min_{\mathbf{X}, \mathbf{U}_1, \mathbf{U}_2, \mathbf{U}_3} \quad & \frac{1}{2} \|\mathbf{U}_3\|_F^2 + p(\mathbf{U}_1) + q(\mathbf{U}_2) \\ \text{s.t.} \quad & \mathbf{X} - \mathbf{U}_1 = 0, \mathbf{X} - \mathbf{U}_2 = 0, \\ & \mathbf{A}\mathbf{X} - \mathbf{Y} - \mathbf{U}_3 = 0, \end{aligned} \quad (10)$$

where  $\mathbf{U}_1 \in R^{m \times n}$ ,  $\mathbf{U}_2 \in R^{m \times n}$ ,  $\mathbf{U}_3 \in R^{L \times n}$ .

The dual of the problem (10) is

$$\begin{aligned} \min_{\mathbf{V}_1, \mathbf{V}_2, \mathbf{V}_3} \quad & p^*(-\mathbf{V}_1) + q^*(-\mathbf{V}_2) + \frac{1}{2} \|\mathbf{V}_3\|_F^2 - \langle \mathbf{V}_3, \mathbf{Y} \rangle \\ \text{s.t.} \quad & -\mathbf{V}_1 - \mathbf{V}_2 - \mathbf{A}^T \mathbf{V}_3 = 0, \end{aligned} \quad (11)$$

where  $\mathbf{V}_1 \in R^{m \times n}$ ,  $\mathbf{V}_2 \in R^{m \times n}$ ,  $\mathbf{V}_3 \in R^{L \times n}$ .

Let  $\sigma > 0$ , the augmented Lagrangian function for the problem (11) is

$$\begin{aligned} L_\sigma(\mathbf{V}_1, \mathbf{V}_2, \mathbf{V}_3; \mathbf{X}) &= p^*(-\mathbf{V}_1) + q^*(-\mathbf{V}_2) + \frac{1}{2} \|\mathbf{V}_3\|_F^2 - \\ &\langle \mathbf{V}_3, \mathbf{Y} \rangle + \frac{\sigma}{2} \|\mathbf{V}_1 + \mathbf{V}_2 + \mathbf{A}^T \mathbf{V}_3 - \sigma^{-1} \mathbf{X}\|_F^2 - \frac{1}{2\sigma} \|\mathbf{X}\|_F^2. \end{aligned}$$

By Proposition 1, the dual sGS-ADMM can be presented in Algorithm 2.

---

### Algorithm 2 A dual sGS-ADMM

---

**Require:** Select an initial point  $(\mathbf{V}_1^0, \mathbf{V}_2^0, \mathbf{V}_3^0; \mathbf{X}^0)$ . Set  $k = 0$ , choose  $\sigma > 0$  and  $\tau \in (0, \frac{1+\sqrt{5}}{2})$ . Iterate the following steps:

**Step 1.** Compute:

$$\begin{aligned} \hat{\mathbf{V}}_3^k &= \underset{\mathbf{V}_3}{\text{argmin}} \left\{ L_\sigma(\mathbf{V}_1^k, \mathbf{V}_2^k, \mathbf{V}_3; \mathbf{X}^k) - \langle \hat{\delta}_{\mathbf{V}_3}^k, \mathbf{V}_3 \rangle \right\}, \\ \mathbf{V}_1^{k+1} &= \underset{\mathbf{V}_1}{\text{argmin}} \left\{ L_\sigma(\mathbf{V}_1, \mathbf{V}_2^k, \hat{\mathbf{V}}_3^k; \mathbf{X}^k) \right\}, \\ \mathbf{V}_3^{k+1} &= \underset{\mathbf{V}_3}{\text{argmin}} \left\{ L_\sigma(\mathbf{V}_1^{k+1}, \mathbf{V}_2^k, \mathbf{V}_3; \mathbf{X}^k) - \langle \delta_{\mathbf{V}_3}^k, \mathbf{V}_3 \rangle \right\}, \\ \mathbf{V}_2^{k+1} &= \underset{\mathbf{V}_2}{\text{argmin}} \left\{ L_\sigma(\mathbf{V}_1^{k+1}, \mathbf{V}_2, \mathbf{V}_3^{k+1}; \mathbf{X}^k) \right\}. \end{aligned}$$

**Step 2.** Update:

$$\mathbf{X}^{k+1} = \mathbf{X}^k - \tau\sigma(-\mathbf{V}_1^{k+1} - \mathbf{V}_2^{k+1} - \mathbf{A}^T \mathbf{V}_3^{k+1}).$$


---

Now we provide the details of Step 1 in Algorithm 2. Finding the minimum of  $L_\sigma(\mathbf{V}_1, \mathbf{V}_2, \mathbf{V}_3; \mathbf{X})$  with respect to  $\mathbf{V}_3$  is equivalent to solving the following problem.

$$\begin{aligned} 0 &= \nabla_{\mathbf{V}_3} L_\sigma(\mathbf{V}_1, \mathbf{V}_2, \mathbf{V}_3; \mathbf{X}) \\ &= \mathbf{V}_3 - \mathbf{Y} + \sigma \mathbf{A}(\mathbf{V}_1 + \mathbf{V}_2 + \mathbf{A}^T \mathbf{V}_3 + \sigma^{-1} \mathbf{X}). \end{aligned}$$

That is, we compute  $\mathbf{V}_3$  by solving the following linear system of equations

$$(\mathbf{I} + \sigma \mathbf{A} \mathbf{A}^T) \mathbf{V}_3 = \mathbf{Y} - \sigma \mathbf{A} \mathbf{V}_1 - \sigma \mathbf{A} \mathbf{V}_2 - \mathbf{A} \mathbf{X}.$$

Making use of the Moreau identity  $\text{Prox}_{\sigma p}(\mathbf{x}) + \sigma \text{Prox}_{p^*/\sigma}(\mathbf{x}/\sigma) = \mathbf{x}$ , we can get  $\mathbf{V}_1, \mathbf{V}_2$  in closed forms as below

$$\mathbf{V}_1 = \frac{1}{\sigma} \text{Prox}_{\sigma p}(\sigma \mathbf{C}_1) - \mathbf{C}_1,$$

$$\mathbf{V}_2 = \frac{1}{\sigma} \text{Prox}_{\sigma q}(\sigma \mathbf{C}_2) - \mathbf{C}_2,$$

where

$$\mathbf{C}_1 = \mathbf{V}_2 + \mathbf{A}^T \mathbf{V}_3 + \sigma^{-1} \mathbf{X},$$

$$\mathbf{C}_2 = \mathbf{V}_1 + \mathbf{A}^T \mathbf{V}_3 + \sigma^{-1} \mathbf{X}.$$

We discuss different cases for different  $p$  and  $q$ .

(i) When  $p(\cdot) = \lambda \|\cdot\|_1 + \delta_{R_+^{m \times n}}(\cdot) + \lambda_{TV} \|\hat{\mathcal{H}}_v(\cdot)\|_1$ , we define  $p_1(\cdot) = \lambda \|\cdot\|_1 + \lambda_{TV} \|\hat{\mathcal{H}}_v(\cdot)\|_1$  for convenience. By [43, Theorem 2] we can obtain the proximal mapping of  $\sigma p$  as

$$\text{Prox}_{\sigma p}(\sigma \mathbf{C}_1) = \Pi_{R_+^{m \times n}}(\text{Prox}_{\sigma p_1}(\sigma \mathbf{C}_1)),$$

where  $\Pi_{R_+^{m \times n}}(\cdot)$  is a projection on  $R_+^{m \times n}$ . We note that the proximal mapping of  $\sigma p_1$  is

$$\text{Prox}_{\sigma p_1}(\sigma \mathbf{C}_1) = \underset{\mathbf{Z}}{\text{argmin}} \left\{ \sigma \lambda \|\mathbf{Z}\|_1 + \sigma \lambda_{TV} \|\hat{\mathcal{H}}_v \mathbf{Z}\|_1 + \frac{1}{2} \|\mathbf{Z} - \sigma \mathbf{C}_1\|_F^2 \right\}.$$

Let

$$\begin{aligned} \mathbf{Z} &= [\mathbf{z}_1, \mathbf{z}_2, \dots, \mathbf{z}_{n_r}, \mathbf{z}_{n_r+1}, \mathbf{z}_{n_r+2}, \dots, \mathbf{z}_{2n_r}, \dots, \\ &\quad \mathbf{z}_{n-n_r+1}, \mathbf{z}_{n-n_r+2}, \dots, \mathbf{z}_n], \\ \mathbf{K} &= [\mathbf{k}_1, \mathbf{k}_2, \dots, \mathbf{k}_{n_r}, \mathbf{k}_{n_r+1}, \mathbf{k}_{n_r+2}, \dots, \mathbf{k}_{2n_r}, \dots, \\ &\quad \mathbf{k}_{n-n_r+1}, \mathbf{k}_{n-n_r+2}, \dots, \mathbf{k}_n], \end{aligned}$$

$$\mathbf{Z}_{\sigma \lambda_{TV}}(\sigma \mathbf{C}_1) := \underset{\mathbf{Z}}{\text{argmin}} \left\{ \sigma \lambda_{TV} \|\hat{\mathcal{H}}_v \mathbf{Z}\|_1 + \frac{1}{2} \|\mathbf{Z} - \sigma \mathbf{C}_1\|_F^2 \right\}, \quad \text{where} \quad (12)$$

where  $\mathbf{K} = \sigma \mathbf{C}_1$  and  $\mathbf{z}_i, \mathbf{k}_i$  ( $i = 1, 2, \dots, n$ ) denote the  $i$ th columns of  $\mathbf{Z}, \mathbf{K}$ . In order to compute  $\mathbf{Z}_{\sigma \lambda_{TV}}(\sigma \mathbf{C}_1)$ , we first denote

$$\begin{aligned} \mathbf{Z}'^* &:= \underset{\mathbf{Z}'}{\text{argmin}} \left\{ \sigma \lambda_{TV} \sum_{k=1}^{n_c-1} \|\mathbf{Z}'(:, k+1) - \mathbf{Z}'(:, k)\|_1 + \right. \\ &\quad \left. \frac{1}{2} \|\mathbf{Z}' - \mathbf{K}'\|_F^2 \right\}, \end{aligned}$$

where

$$\begin{aligned} \mathbf{Z}' &:= \begin{pmatrix} \mathbf{z}_1 & \mathbf{z}_{n_r+1} & \dots & \mathbf{z}_{n-n_r+1} \\ \mathbf{z}_2 & \mathbf{z}_{n_r+2} & \dots & \mathbf{z}_{n-n_r+2} \\ \vdots & \vdots & \ddots & \vdots \\ \mathbf{z}_{n_r} & \mathbf{z}_{2n_r} & \dots & \mathbf{z}_n \end{pmatrix}, \\ \mathbf{K}' &:= \begin{pmatrix} \mathbf{k}_1 & \mathbf{k}_{n_r+1} & \dots & \mathbf{k}_{n-n_r+1} \\ \mathbf{k}_2 & \mathbf{k}_{n_r+2} & \dots & \mathbf{k}_{n-n_r+2} \\ \vdots & \vdots & \ddots & \vdots \\ \mathbf{k}_{n_r} & \mathbf{k}_{2n_r} & \dots & \mathbf{k}_n \end{pmatrix}, \\ \mathbf{Z}'^* &:= \begin{pmatrix} \mathbf{z}_1^* & \mathbf{z}_{n_r+1}^* & \dots & \mathbf{z}_{n-n_r+1}^* \\ \mathbf{z}_2^* & \mathbf{z}_{n_r+2}^* & \dots & \mathbf{z}_{n-n_r+2}^* \\ \vdots & \vdots & \ddots & \vdots \\ \mathbf{z}_{n_r}^* & \mathbf{z}_{2n_r}^* & \dots & \mathbf{z}_n^* \end{pmatrix}. \end{aligned}$$

Since  $\mathbf{Z}'^*$  is separable, we can find  $\mathbf{Z}'^*$  row by row. That is,

$$\begin{aligned} \mathbf{Z}'^*(i, :) &= \underset{\mathbf{Z}'(i, :)}{\text{argmin}} \left\{ \sigma \lambda_{TV} \sum_{k=1}^{n_c-1} |\mathbf{Z}'(i, k+1) - \mathbf{Z}'(i, k)| + \right. \\ &\quad \left. \frac{1}{2} \|\mathbf{Z}'(i, :) - \mathbf{K}'(i, :)\|_2^2 \right\}, \quad i = 1, 2, \dots, m \times n_r. \end{aligned}$$

In our numerical experiments, we use Condat's algorithm [39] to compute  $\mathbf{Z}'^*$ . Then we can obtain  $\mathbf{Z}_{\sigma \lambda_{TV}}(\sigma \mathbf{C}_1)$  from  $\mathbf{Z}'^*$  easily as below

$$\begin{aligned} \mathbf{Z}_{\sigma \lambda_{TV}}(\sigma \mathbf{C}_1) &= [\mathbf{z}_1^*, \mathbf{z}_2^*, \dots, \mathbf{z}_{n_r}^*, \mathbf{z}_{n_r+1}^*, \mathbf{z}_{n_r+2}^*, \dots, \mathbf{z}_{2n_r}^*, \\ &\quad \dots, \mathbf{z}_{n-n_r+1}^*, \mathbf{z}_{n-n_r+2}^*, \dots, \mathbf{z}_n^*]. \end{aligned}$$

By Proposition 2 in [40] we can compute the proximal mapping of  $\sigma p_1$  as below

$$\begin{aligned} \text{Prox}_{\sigma p_1}(\sigma \mathbf{C}_1) &= \text{Prox}_{\sigma \lambda \|\cdot\|_1}(\mathbf{Z}_{\sigma \lambda_{TV}}(\sigma \mathbf{C}_1)) \\ &= \text{sign}(\mathbf{Z}_{\sigma \lambda_{TV}}(\sigma \mathbf{C}_1)) \circ \max(|\mathbf{Z}_{\sigma \lambda_{TV}}(\sigma \mathbf{C}_1)| - \sigma \lambda \mathbf{1}, \mathbf{0}). \end{aligned}$$

In the light of Proposition 2 in [40], we can compute the proximal mapping of  $\sigma p_1$  by composing the proximal mapping of  $\sigma \lambda \|\cdot\|_1$  with the proximal mapping of  $\sigma \lambda_{TV} \|\hat{\mathcal{H}}_v(\cdot)\|_1$ .

(ii) When  $p(\cdot) = \lambda \|\cdot\|_{2,1} + \delta_{R_+^{m \times n}}(\cdot) + \lambda_{TV} \|\hat{\mathcal{H}}_v(\cdot)\|_1$ , we let  $p_2(\cdot) = \lambda \|\cdot\|_{2,1} + \lambda_{TV} \|\hat{\mathcal{H}}_v(\cdot)\|_1$ . Similarly to (i), we can compute

$$\text{Prox}_{\sigma p}(\sigma \mathbf{C}_1) = \Pi_{R_+^{m \times n}}(\text{Prox}_{\sigma p_2}(\sigma \mathbf{C}_1)).$$

Based on Corollary 4 in [43], the proximal mapping of  $\sigma p_2$  takes the following form

$$\text{Prox}_{\sigma p_2}(\sigma \mathbf{C}_1) = \text{diag}(\alpha_1, \alpha_2, \dots, \alpha_m) \mathbf{Z}_{\sigma \lambda_{TV}}(\sigma \mathbf{C}_1),$$

$$\alpha_i = \left( \frac{\max\{\|\mathbf{Z}_{\sigma \lambda_{TV}}(\sigma \mathbf{C}_1)(i, :)\|_2 - \sigma \lambda, 0\}}{\max\{\|\mathbf{Z}_{\sigma \lambda_{TV}}(\sigma \mathbf{C}_1)(i, :)\|_2 - \sigma \lambda, 0\} + \sigma \lambda} \right)$$

and  $\text{diag}(\alpha_1, \alpha_2, \dots, \alpha_m)$  denotes the diagonal matrix with diagonal entries  $\alpha_1, \alpha_2, \dots, \alpha_m$ .

(iii) Note  $q(\cdot) = \lambda_{TV} \|\hat{\mathcal{H}}_h(\cdot)\|_1$ , let

$$\begin{aligned} \mathbf{Z}''^* &:= \underset{\mathbf{Z}''}{\text{argmin}} \left\{ \sigma \lambda_{TV} \sum_{k=1}^{n_r-1} \|\mathbf{Z}''(:, k+1) - \mathbf{Z}''(:, k)\|_1 + \right. \\ &\quad \left. \frac{1}{2} \|\mathbf{Z}'' - \mathbf{K}''\|_F^2 \right\}, \end{aligned}$$

where

$$\begin{aligned} \mathbf{Z}'' &:= \begin{pmatrix} \mathbf{z}_1 & \mathbf{z}_2 & \dots & \mathbf{z}_{n_r} \\ \mathbf{z}_{n_r+1} & \mathbf{z}_{n_r+2} & \dots & \mathbf{z}_{2n_r} \\ \vdots & \vdots & \ddots & \vdots \\ \mathbf{z}_{n-n_r+1} & \mathbf{z}_{n-n_r+2} & \dots & \mathbf{z}_n \end{pmatrix}, \\ \mathbf{K}'' &:= \begin{pmatrix} \mathbf{k}_1 & \mathbf{k}_2 & \dots & \mathbf{k}_{n_r} \\ \mathbf{k}_{n_r+1} & \mathbf{k}_{n_r+2} & \dots & \mathbf{k}_{2n_r} \\ \vdots & \vdots & \ddots & \vdots \\ \mathbf{k}_{n-n_r+1} & \mathbf{k}_{n-n_r+2} & \dots & \mathbf{k}_n \end{pmatrix}, \\ \mathbf{Z}''^* &:= \begin{pmatrix} \mathbf{z}_1^* & \mathbf{z}_2^* & \dots & \mathbf{z}_{n_r}^* \\ \mathbf{z}_{n_r+1}^* & \mathbf{z}_{n_r+2}^* & \dots & \mathbf{z}_{2n_r}^* \\ \vdots & \vdots & \ddots & \vdots \\ \mathbf{z}_{n-n_r+1}^* & \mathbf{z}_{n-n_r+2}^* & \dots & \mathbf{z}_n^* \end{pmatrix}. \end{aligned}$$

Then we can compute  $\mathbf{Z}''^*$  similarly to that of  $\mathbf{Z}'^*$ , that is,

$$\begin{aligned} \mathbf{Z}''^*(i, :) &= \underset{\mathbf{Z}''(i, :)}{\text{argmin}} \left\{ \sigma \lambda_{TV} \sum_{k=1}^{n_r-1} |\mathbf{Z}''(i, k+1) - \mathbf{Z}''(i, k)| + \right. \\ &\quad \left. \frac{1}{2} \|\mathbf{Z}''(i, :) - \mathbf{K}''(i, :)\|_2^2 \right\}, \quad i = 1, 2, \dots, m \times n_c. \end{aligned}$$

We can obtain the proximal mapping of  $\sigma q$  from  $\mathbf{Z}''^*$  as below

$$\begin{aligned} \text{Prox}_{\sigma q}(\sigma \mathbf{C}_1) &= [\mathbf{z}_1^*, \mathbf{z}_2^*, \dots, \mathbf{z}_{n_r}^*, \mathbf{z}_{n_r+1}^*, \mathbf{z}_{n_r+2}^*, \dots, \mathbf{z}_{2n_r}^*, \\ &\quad \dots, \mathbf{z}_{n-n_r+1}^*, \mathbf{z}_{n-n_r+2}^*, \dots, \mathbf{z}_n^*]. \end{aligned}$$

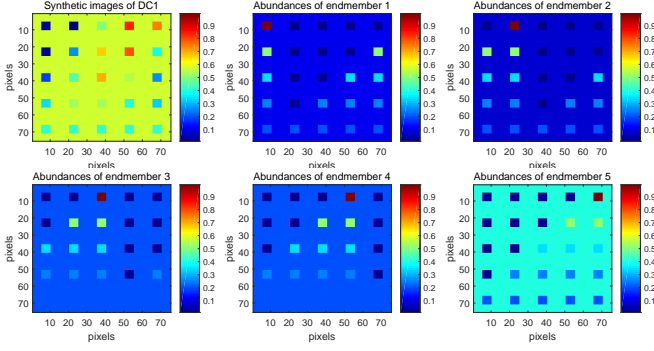


Fig. 1. The synthetic images of DC1 and the true abundances of each endmember in the simulated data cube 1.

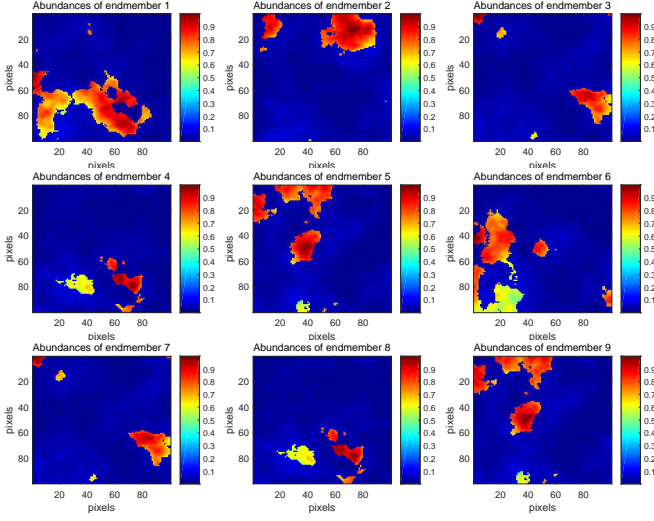


Fig. 2. The true abundances of each endmember in the simulated data cube 2.

### B. Convergence analysis

In this subsection, we analyze the global convergence and the local linear convergence rate of the dual sGS-ADMM. Note that the problem (11) can also be written in the following form

$$\begin{aligned} \min_{\mathbf{W}, \mathbf{V}_2} \quad & \psi(\mathbf{W}) + \varphi(\mathbf{V}_2) \\ \text{s.t.} \quad & -\mathcal{A}\mathbf{W} - \mathbf{V}_2 = 0, \end{aligned} \quad (13)$$

where  $\mathbf{W} = (\mathbf{V}_1^T, \mathbf{V}_3^T)^T \in R^{(m+L) \times n}$ ,  $\mathcal{A} = [\mathbf{I}_{m \times m}, \mathbf{A}^T]$  and

$$\begin{aligned} \psi(\mathbf{W}) &= p^*(-\mathbf{V}_1) + \frac{1}{2} \|\mathbf{V}_3\|_F^2 - \langle \mathbf{V}_3, \mathbf{Y} \rangle, \\ \varphi(\mathbf{V}_2) &= q^*(-\mathbf{V}_2). \end{aligned}$$

Suppose that  $(\mathbf{W}, \mathbf{V}_2) \in R^{(m+L) \times n} \times R^{m \times n}$  is an optimal solution to the problem (13). If there exists  $\mathbf{X} \in R^{m \times n}$  such that  $(\mathbf{W}, \mathbf{V}_2, \mathbf{X})$  satisfies the following KKT system

$$\begin{cases} 0 \in \partial\psi(\mathbf{W}) + \mathcal{A}^* \mathbf{X}, \\ 0 \in \partial\varphi(\mathbf{V}_2) + \mathbf{X}, \\ -\mathcal{A}\mathbf{W} - \mathbf{V}_2 = 0, \end{cases} \quad (14)$$

then  $(\mathbf{W}, \mathbf{V}_2, \mathbf{X})$  is a KKT point for the problem (13). Let  $\bar{\Omega}$  be the solution set of the KKT system (14) for convenience. Let  $\mathcal{E} : R^{m \times n} \rightarrow R^{(m+L) \times n} \times R^{m \times n}$  be a linear operator

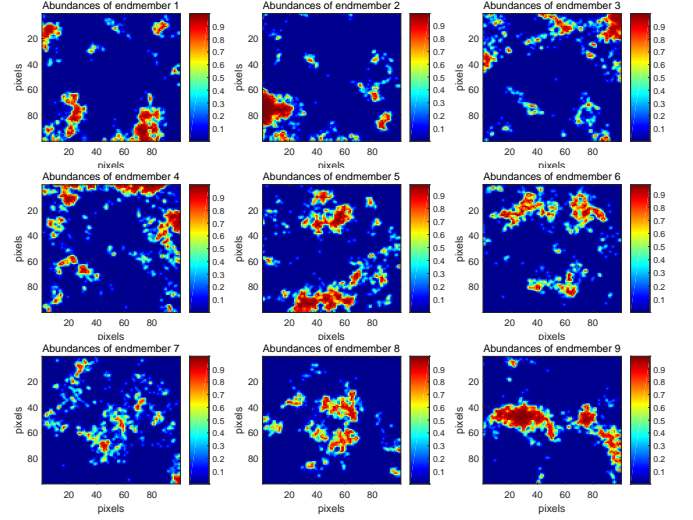


Fig. 3. The true abundances of each endmember in the simulated data cube 3.

such that its adjoint  $\mathcal{E}^*(\mathbf{W}, \mathbf{V}_2) = -\mathcal{A}\mathbf{W} - \mathbf{V}_2$ . For  $\mathbf{v} := (\mathbf{W}, \mathbf{V}_2, \mathbf{X})$ , the KKT mapping is defined by

$$\mathbf{R}(\mathbf{v}) := \begin{pmatrix} \mathbf{W} - \text{Prox}_{\psi}(\mathbf{W} - \mathcal{A}^* \mathbf{X}) \\ \mathbf{V}_2 - \text{Prox}_{\varphi}(\mathbf{X} - \mathbf{V}_2) \\ -\mathcal{A}\mathbf{W} - \mathbf{V}_2 \end{pmatrix}.$$

Since the subdifferential mappings of the closed proper convex functions  $p^*$  and  $q^*$  are maximally monotone [37, Theorem 12.17], there exist two self-adjoint and positive semidefinite linear operators  $\Sigma_{\psi}$  and  $\Sigma_{\varphi}$  such that for all  $\mathbf{y}, \mathbf{y}' \in \text{dom}(\psi)$ ,  $\xi \in \partial\psi(\mathbf{y})$  and  $\xi' \in \partial\psi(\mathbf{y}')$

$$\psi(\mathbf{y}) \geq \psi(\mathbf{y}') + \langle \xi', \mathbf{y} - \mathbf{y}' \rangle + \frac{1}{2} \|\mathbf{y} - \mathbf{y}'\|_{\Sigma_{\psi}}^2,$$

$$\langle \xi - \xi', \mathbf{y} - \mathbf{y}' \rangle \geq \|\mathbf{y} - \mathbf{y}'\|_{\Sigma_{\psi}}^2,$$

and for all  $\mathbf{z}, \mathbf{z}' \in \text{dom}(\varphi)$ ,  $\zeta \in \partial\varphi(\mathbf{z})$  and  $\zeta' \in \partial\varphi(\mathbf{z}')$

$$\varphi(\mathbf{z}) \geq \varphi(\mathbf{z}') + \langle \zeta', \mathbf{z} - \mathbf{z}' \rangle + \frac{1}{2} \|\mathbf{z} - \mathbf{z}'\|_{\Sigma_{\varphi}}^2,$$

$$\langle \zeta - \zeta', \mathbf{z} - \mathbf{z}' \rangle \geq \|\mathbf{z} - \mathbf{z}'\|_{\Sigma_{\varphi}}^2.$$

For the convergence of the dual sGS-ADMM, we need the following constraint qualification.

*Assumption 2:* The KKT system (14) has a non-empty solution set.

We can also obtain the global convergence and linear convergence rate of the sGS-ADMM based on [28, Theorem B.1] and [29, Theorem 2].

*Theorem 2:* Suppose that Assumption 2 holds and  $\mathbf{T} := (\sigma^{-1} \mathbf{I} + \mathbf{A} \mathbf{A}^T) - \mathbf{A} [\mathbf{I} + \mathbf{A}^T (\sigma^{-1} \mathbf{I} + \mathbf{A} \mathbf{A}^T)^{-1} \mathbf{A}]^{-1} \mathbf{A}^T$  is positive definite. Let  $\tau \in (0, \frac{1+\sqrt{5}}{2})$ , then there exists a KKT point  $\bar{\mathbf{v}} := (\bar{\mathbf{W}}, \bar{\mathbf{V}}_2, \bar{\mathbf{X}}) \in \bar{\Omega}$  such that the sequence  $\{(\mathbf{V}_1^k, \mathbf{V}_2^k, \mathbf{V}_3^k, \mathbf{X}^k)\}$  generated by Algorithm 2 converges to  $\bar{\mathbf{v}}$ . Assume that  $\mathbf{R}^{-1}$  is calm at the origin for  $\bar{\mathbf{v}}$  with modulus  $\eta' > 0$ , i.e., there exists  $r' > 0$  such that

$$\text{dist}(\mathbf{u}, \bar{\Omega}) \leq \eta' \|\mathbf{R}(\mathbf{u})\|, \quad \forall \mathbf{u} \in \{\mathbf{u} : \|\mathbf{u} - \bar{\mathbf{u}}\| \leq r'\}.$$

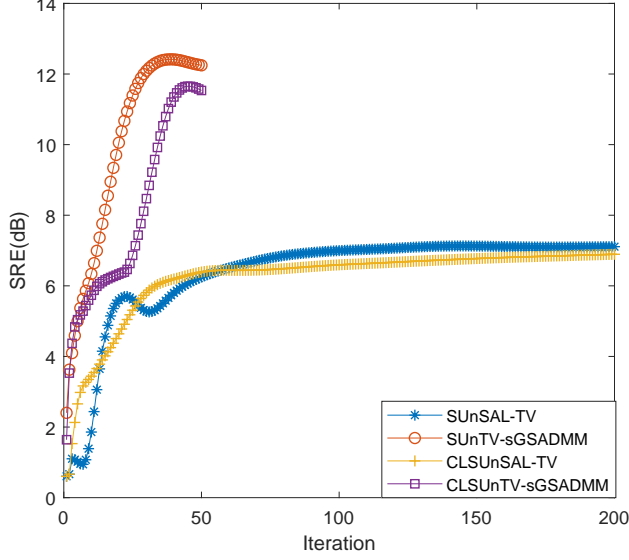


Fig. 4. Variations of the SRE(dB) values with respect to the iterations for different algorithms when dealing with the DC1 with white noise (SNR = 20 dB).

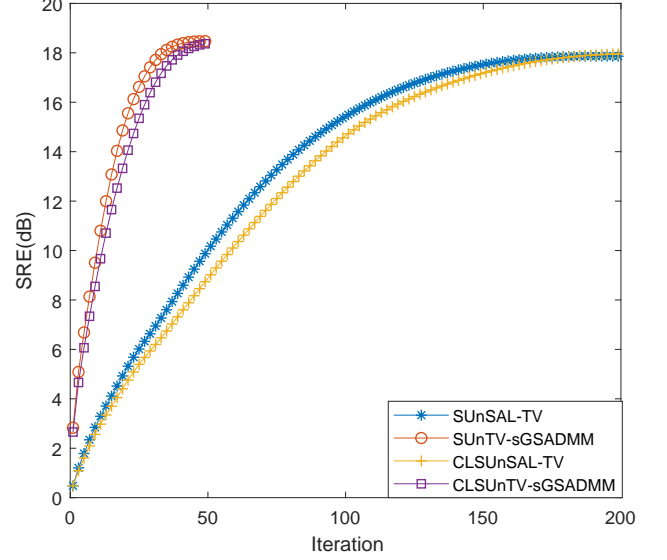


Fig. 5. Variations of the SRE(dB) values with respect to the iterations for different algorithms when dealing with the DC2 with correlated noise (SNR = 20 dB).

Then there exists an integer  $\bar{k}' \geq 1$  such that for all  $k' \geq \bar{k}'$ ,

$$\text{dist}_{\mathcal{P}}^2(\mathbf{u}^{k+1}, \bar{\Omega}) \leq \mu' \text{dist}_{\mathcal{P}}^2(\mathbf{u}^k, \bar{\Omega}),$$

where  $\mu' \in (0, 1)$ ,

$$\mathcal{P} := \text{Diag}(\mathcal{T} + \Sigma_{\psi}, \Sigma_{\varphi} + \sigma \mathcal{I}, (\tau \sigma)^{-1} \mathcal{I}) + s_{\tau} \sigma \mathcal{E} \mathcal{E}^*,$$

and

$$s_{\tau} := \frac{5 - \tau - 3\min\{\tau, \tau^{-1}\}}{4}.$$

Moreover, there exists a positive number  $\zeta' \in [\mu', 1)$  such that for all  $k' \geq 1$

$$\text{dist}_{\mathcal{P}}^2(\mathbf{u}^{k+1}, \bar{\Omega}) \leq \zeta' \text{dist}_{\mathcal{P}}^2(\mathbf{u}^k, \bar{\Omega}).$$

*Proof:* See Appendix B.  $\square$

*Remark 2:* For the case of  $\rho = 1$  in the problem (3),  $p$  and  $q$  are piecewise linear-quadratic functions. We also know that the calmness condition holds automatically by [34, Proposition 2.24] and [35, Corollary].

## VI. NUMERICAL RESULTS WITH THE SIMULATED DATA

In this section, we implement some numerical experiments to demonstrate the efficiency of our algorithm. All the experiments were conducted on a PC with Inter (R) Core (TM) i5-4210M CPU @2.60GHz 2.59GHz of 8G memory running 64bit Windows operation system. All the codes were written in MATLAB 2017b with some subroutines in C. For convenience, we use SUnTV-sGSADMM and CLSUnTV-sGSADMM to denote the dual sGS-ADMM applied to the SUnTV and CLSUnTV, respectively. The MATLAB codes of SUnSAL-TV and CLSUnSAL-TV are based on [15].<sup>2</sup>

<sup>2</sup>downloaded from <http://www.lx.it.pt/~bioucas/publications.html>.

We use the signal reconstruction error (SRE) to measure the performances of different algorithms, which is defined as follows [14]:

$$\text{SRE(dB)} = 10 \log_{10} \frac{E[\|\mathbf{x}\|_2^2]}{E[\|\mathbf{x} - \hat{\mathbf{x}}\|_2^2]},$$

where  $\mathbf{x}$  and  $\hat{\mathbf{x}}$  denote the true abundances and the estimated abundances, respectively and  $E[\cdot]$  represents the statistical expectation. In general, a larger SRE indicates a better unmixing performance. In addition, the probability of success ( $p_s$ ) is also employed to estimate the probability that the relative error power is less than a certain threshold value [14]:

$$p_s = P(\|\hat{\mathbf{x}} - \mathbf{x}\|^2 / \|\mathbf{x}\|^2 \leq \text{threshold}).$$

The unmixing algorithm can be regarded as being successful when  $\|\hat{\mathbf{x}} - \mathbf{x}\|^2 / \|\mathbf{x}\|^2 \leq 0.316(5 \text{ dB})$  in all our experiments.

We measure the accuracy of the solutions by the following relative KKT residual and Error:

$$\begin{aligned} \mathbf{R}_{P_1} &= (\|\mathbf{D}_1 - \mathbf{A}\tilde{\mathbf{D}}\|_F + \|\mathbf{D}_2 - \tilde{\mathbf{D}}\|_F + \|\mathbf{D}_3 - \tilde{\mathbf{D}}\|_F \\ &\quad \|\mathbf{D}_4 - \mathcal{H}\mathbf{D}_3\|_F + \|\mathbf{D}_5 - \tilde{\mathbf{D}}\|_F) / (1 + \|\mathbf{A}\|_F), \\ \mathbf{R}_{D_1} &= (\|\mathbf{A}^T \mathbf{\Lambda}_1 + \mathbf{\Lambda}_2 + \mathbf{\Lambda}_3 + \mathbf{\Lambda}_5\|_F + \\ &\quad \|\mathbf{\Lambda}_3 - \mathcal{H}^T \mathbf{\Lambda}_4\|_F) / (1 + \|\mathbf{A}\|_F), \\ \text{Error}_1 &= \|\tilde{\mathbf{D}}^{k+1} - \tilde{\mathbf{D}}^k\|_F / \|\tilde{\mathbf{D}}^{k+1}\|_F, \\ \mathbf{R}_{P_2} &= \|\mathbf{A}\mathbf{X} - \mathbf{Y} - \mathbf{U}_3\|_F / (1 + \|\mathbf{Y}\|_F), \\ \mathbf{R}_{D_2} &= \|\mathbf{V}_1 + \mathbf{V}_2 + \mathbf{A}^T \mathbf{V}_3\|_F / (1 + \|\mathbf{A}\|_F), \\ \text{Error}_2 &= \|\mathbf{X}^{k+1} - \mathbf{X}^k\|_F / \|\mathbf{X}^{k+1}\|_F. \end{aligned}$$

The stopping criterion for Algorithm 1 is  $\mathbf{R}_{P_1} < \text{tol}_1$  and  $\mathbf{R}_{D_1} < \text{tol}_1$  or  $\text{Error}_1 < \text{tol}_2$ , and the stopping criterion for Algorithm 2 is  $\mathbf{R}_{P_2} < \text{tol}_1$  and  $\mathbf{R}_{D_2} < \text{tol}_1$  or  $\text{Error}_2 < \text{tol}_2$ , where  $\text{tol}_1$  and  $\text{tol}_2$  are predefined error tolerances. In our implementation, we empirically set  $\text{tol}_1 = 10^{-3}$  and

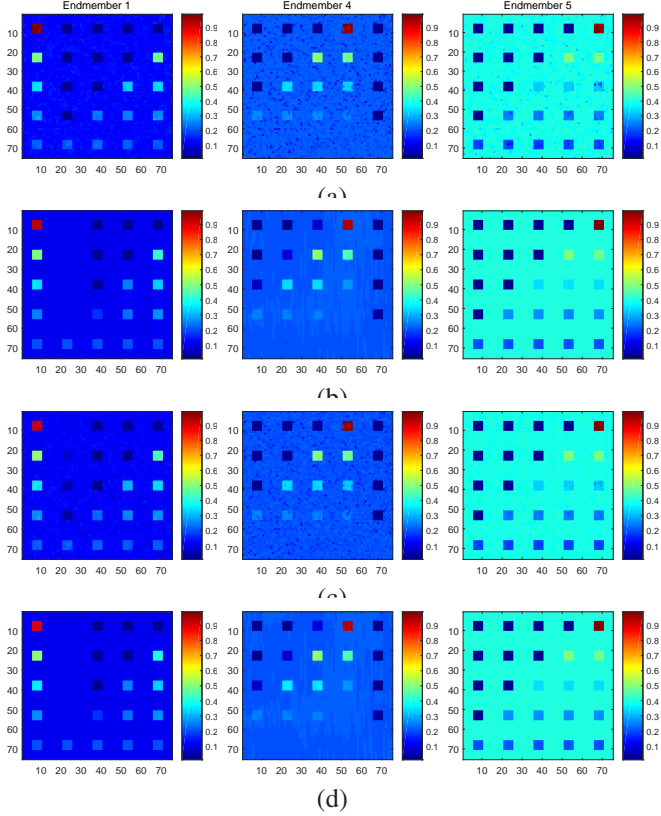


Fig. 6. The estimated abundances obtained by the different unmixing algorithms for endmember 1, endmember 4, endmember 5 in the DC1 with SNR = 30 dB (correlated noise). From top to bottom: (a) SUnSAL-TV, (b) SUnTV-sGSADMM, (c) CLSUnSAL-TV, (d) CLSUnTV-sGSADMM.

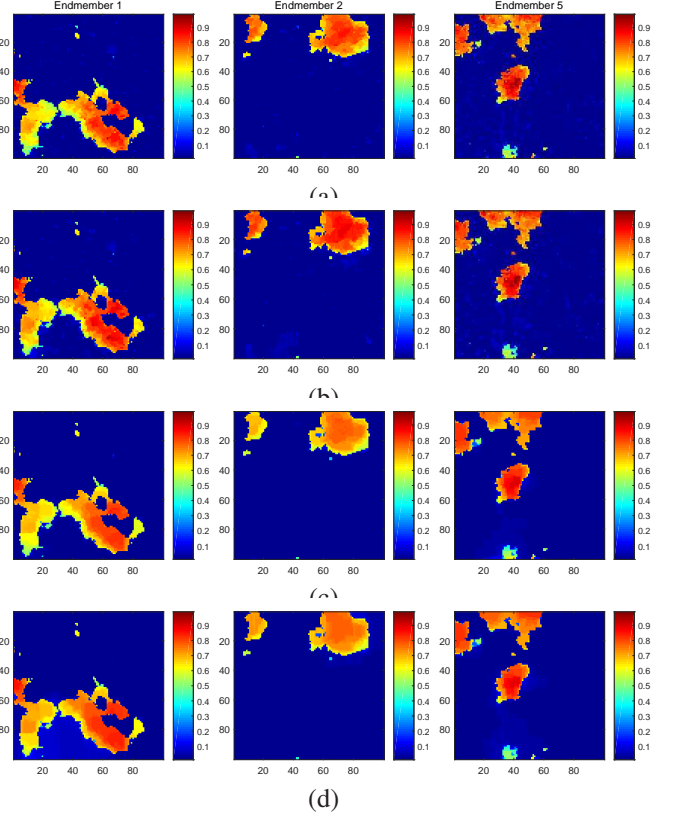


Fig. 7. The estimated abundances obtained by the different unmixing algorithms for endmember 1, endmember 2, and endmember 5 in the DC2 with SNR = 20 dB (white noise). From top to bottom: (a) SUnSAL-TV, (b) SUnTV-sGSADMM, (c) CLSUnSAL-TV, (d) CLSUnTV-sGSADMM.

$\text{tol}_2 = 10^{-4}$ . The maximum number of iterations of the SUnSAL-TV and CLSUnSAL-TV are capped by 200, and the maximum number of iterations of the SUnTV-sGSADMM and CLSUnTV-sGSADMM are capped by 50.<sup>3</sup>

The algorithms are tested using different values of the parameters  $\lambda$  and  $\lambda_{TV}$  in a finite set  $\{0.5, 0.1, 0.05, 0.01, 0.005, 0.001, 0.0005, 0.0001\}$ .

For the simulated data experiments, the spectral library  $\mathbf{A} \in \mathbb{R}^{224 \times 240}$  is randomly picked out from the United States Geological Survey (USGS) digital spectral library splib06.<sup>4</sup> These spectra have 224 bands and are uniformly distributed between 0.4-2.5  $\mu\text{m}$ . The mutual coherence of  $\mathbf{A}$  is very close to 1. By using this spectral library, we generated the following three simulated hyperspectral data cubes.

(1) Simulated Data Cube 1 (DC1): The size of the DC1 is  $75 \times 75$ , and each pixel contains 224 bands. We randomly chose five endmembers from  $\mathbf{A}$  and generated the abundances of endmembers following the methodology of [14]. Fig. 1 shows the synthetic images and the true abundance maps of each endmembers. Then the white noise and the correlated noise (resulting from low-pass filtering i.i.d. Gaussian noise, using a normalized cutoff frequency of  $5\pi/L$ ) with signal-to-noise

ratio ( $\text{SNR} = E[\|\mathbf{Ax}\|_2^2]/E[\|\mathbf{n}\|_2^2]$ ) of 20 dB, 30 dB and 40 dB were added to the DC1, respectively.

(2) Simulated Data Cube 2 (DC2): The size of the DC2 is  $100 \times 100$ , and each pixel contains 224 bands. 9 endmembers were randomly chosen from  $\mathbf{A}$ . The abundances of the DC2 satisfy the ANC and the ASC, and it was generated based on the Gaussian fields method whose type is Mattern [42]. As shown in Fig. 2, the abundance maps of each endmembers in the DC2 are more smooth than that in the DC1. Similar to the DC1, the white noise and the correlated noise were added to the DC2 with different SNR.

(3) Simulated Data Cube 3 (DC3): The way we generated the DC3 is like the way of generating the DC2 in [15]. Similarly, 9 endmembers were randomly chosen from  $\mathbf{A}$ , and the abundances of each endmembers satisfy the ANC and the ASC. The true abundance maps of each endmembers in the DC3 are shown in Fig. 3. Similar to the DC1 and DC2, the white noise and the correlated noise were added to the DC3.

In Table I and Table II, we report the SRE,  $p_s$ , the computing time and the optimal parameters for the different unmixing algorithms under different SNR levels. As can be seen in Table I and Table II, with regard to the DC1, the unmixing based on the dual sGS-ADMM is 8 to 9 times faster than that based on the pADMM in the white noise case; while the unmixing based on the dual sGS-ADMM is 9 to 10 times faster than that based on the pADMM in the correlated noise case. For the DC2 and the DC3, both the SUnTV-sGSADMM and the

<sup>3</sup>Since the SRE value will get worse after the KKT residual is smaller than some value, and Algorithm 2 is obviously faster than Algorithm 1 according to the experiments behind, the settings of the maximal iterations are not the same.

<sup>4</sup>Available online: <http://speclab.cr.usgs.gov/spectral.lib06>.

TABLE I

THE SRE VALUES, THE  $p_s$  VALUES, THE RUNNING TIME AND THE REGULARIZATION PARAMETERS OF THE DIFFERENT UNMIXING ALGORITHMS FOR THE SIMULATED DATA (WHITE NOISE)

White noise						
Data cube	SNR(dB)	Parameters	SUnSAL-TV	SUnTV-sGSADMM	CLSUnSAL-TV	CLSUnTV-sGSADMM
DC1	20	SRE(dB)	7.11	12.25	6.89	11.53
		$p_s$	0.96	0.9778	0.9495	0.9733
		time(s)	141.8	15.5	141.3	16.3
		$\lambda$	0.05	0.005	0.5	0.5
		$\lambda_{TV}$	0.05	0.1	0.05	0.1
	30	SRE(dB)	15.11	17.28	14.19	16.39
		$p_s$	0.9956	0.9956	0.9956	1
		time(s)	145.9	16.5	141.7	16.2
		$\lambda$	0.005	0.001	0.5	0.1
		$\lambda_{TV}$	0.01	0.01	0.01	0.01
	40	SRE(dB)	22.38	23.25	22.80	23.16
		$p_s$	1	1	1	1
		time(s)	141.6	15.4	141.3	15.9
		$\lambda$	0.001	0.001	0.1	0.1
		$\lambda_{TV}$	0.005	0.005	0.005	0.005
DC2	20	SRE(dB)	8.67	8.98	6.98	7.17
		$p_s$	0.8485	0.8832	0.7741	0.7639
		time(s)	212.2	28.4	208.6	28.1
		$\lambda$	0.01	0.01	0.0005	0.0005
		$\lambda_{TV}$	0.01	0.01	0.05	0.05
	30	SRE(dB)	15.92	16.22	14.33	14.4
		$p_s$	0.9967	0.9942	0.9939	0.9917
		time(s)	210.3	28.2	209.4	28.5
		$\lambda$	0.005	0.005	0.005	0.0001
		$\lambda_{TV}$	0.005	0.005	0.005	0.005
	40	SRE(dB)	21.08	21.68	19.78	19.8
		$p_s$	0.9998	0.9998	0.9999	0.9998
		time(s)	207.6	28.2	210.9	28.7
		$\lambda$	0.001	0.0005	0.01	0.005
		$\lambda_{TV}$	0.001	0.001	0.001	0.001
DC3	20	SRE(dB)	5.88	6.23	5.12	5.14
		$p_s$	0.6386	0.6699	0.595	0.582
		time(s)	212.4	29.5	213.8	29.3
		$\lambda$	0.01	0.01	0.001	0.001
		$\lambda_{TV}$	0.01	0.01	0.05	0.05
	30	SRE(dB)	11.65	11.64	9.72	9.67
		$p_s$	0.953	0.9451	0.9025	0.8904
		time(s)	209.2	29.2	212.2	29.7
		$\lambda$	0.01	0.005	0.05	0.0001
		$\lambda_{TV}$	0.005	0.005	0.005	0.005
	40	SRE(dB)	18.05	17.9	15.9	15.96
		$p_s$	0.9999	0.9996	0.9982	0.9954
		time(s)	211.3	29.5	211.5	29.9
		$\lambda$	0.005	0.001	0.005	0.0001
		$\lambda_{TV}$	0.0005	0.0005	0.001	0.001

CLSUnTV-sGSADMM are about 7 to 8 times faster than the SUnSAL-TV and the CLSUnSAL-TV for both the white noise and the correlated noise under different SNR levels.

Furthermore, we can see that almost all the SRE values and the  $p_s$  values based on the dual sGS-ADMM are relatively higher than those based on the pADMM. Especially for the DC1, the SRE value by the SUnTV-sGSADMM increases by more than 5 dB compared with that by the SUnSAL-TV in the Gaussian noise case with SNR=20 dB. And in the correlated noise case with SNR=20 dB, the computing time of the CLSUnTV-sGSADMM is only one ninth of the CLSUnSAL-TV, meanwhile its SRE value has increased by nearly 6 dB. Fig. 4 and Fig. 5 show the variations of the SRE(dB) values with respect to the iterations obtained by the different unmixing algorithms. From Fig. 4 and Fig. 5, we can see that the SRE value of the unmixing based on the dual sGS-

ADMM can reach its peak value within 50 iterations, while the SRE value of the unmixing based on the pADMM can reach its peak value in 200 iterations. The peak SRE value of the unmixing based on the pADMM is obviously lower than that based on the dual sGS-ADMM in Fig. 4, and the peak SRE value of the unmixing based on the pADMM is close to that based on the dual sGS-ADMM in Fig. 5.

For visual comparison, Fig. 6 shows the estimated abundances obtained by the different unmixing algorithms for endmember 1, endmember 4, and endmember 5 in the DC1 with SNR = 20 dB (correlated noise). Fig. 7 and Fig. 8 show the estimated abundances obtained by the different unmixing algorithms for endmember 1, endmember 2, and endmember 5 in the DC2 and for endmember 1, endmember 4, and endmember 5 in the DC3 with SNR=20 dB (white noise), respectively. The estimated abundances shown in Fig. 6, Fig.

TABLE II

THE SRE VALUES, THE  $p_s$  VALUES, THE RUNNING TIME AND THE REGULARIZATION PARAMETERS OF THE DIFFERENT UNMIXING ALGORITHMS FOR THE SIMULATED DATA (CORRELATED NOISE)

Correlated noise						
Data cube	SNR(dB)	Parameters	SUnSAL-TV	SUnTV-sGSADMM	CLSUnSAL-TV	CLSUnTV-sGSADMM
DC1	20	SRE(dB)	12.26	18.37	12.25	18.26
		$p_s$	0.9964	0.9993	0.9993	1
		time(s)	138.3	14.6	139.4	14.3
		$\lambda$	0.005	0.001	0.1	0.1
		$\lambda_{TV}$	0.0001	0.01	0.0001	0.01
	30	SRE(dB)	21.14	23.77	21.06	22.86
		$p_s$	1	1	1	1
		time(s)	137.8	15.1	137.9	16.1
		$\lambda$	0.001	0.0005	0.1	0.05
		$\lambda_{TV}$	0.0001	0.001	0.0001	0.0001
	40	SRE(dB)	30.93	33.90	30.75	31.94
		$p_s$	1	1	1	1
		time(s)	133.6	15.3	135.8	15.4
		$\lambda$	0.0005	0.0001	0.01	0.01
		$\lambda_{TV}$	0.0001	0.0005	0.0001	0.0005
DC2	20	SRE(dB)	17.86	18.47	17.96	18.38
		$p_s$	1	1	1	1
		time(s)	208.7	30.1	210.1	29.1
		$\lambda$	0.0005	0.0005	0.01	0.0005
		$\lambda_{TV}$	0.0001	0.0001	0.0001	0.0001
	30	SRE(dB)	24.82	25.25	25.42	25.87
		$p_s$	1	1	1	0.9999
		time(s)	210.2	30.6	211.6	29.7
		$\lambda$	0.0005	0.0005	0.01	0.005
		$\lambda_{TV}$	0.0001	0.0001	0.0001	0.0005
	40	SRE(dB)	27.01	27.28	27.97	28.3
		$p_s$	1	1	0.9999	0.9999
		time(s)	216.6	29.3	214.8	28.8
		$\lambda$	0.0005	0.0005	0.01	0.005
		$\lambda_{TV}$	0.0001	0.0001	0.0005	0.0005
DC3	20	SRE(dB)	16.25	17.49	16.13	17.38
		$p_s$	0.9955	0.9989	0.9917	0.9995
		time(s)	210.8	29.4	216.3	30.3
		$\lambda$	0.001	0.001	0.01	0.0005
		$\lambda_{TV}$	0.0001	0.0001	0.0001	0.0001
	30	SRE(dB)	25.1	26.76	24.41	25.39
		$p_s$	1	1	1	1
		time(s)	212.5	29.4	214.2	30.1
		$\lambda$	0.0005	0.0005	0.01	0.0005
		$\lambda_{TV}$	0.0001	0.0001	0.0001	0.0001
	40	SRE(dB)	31.79	33.24	29.99	29.78
		$p_s$	1	1	1	1
		time(s)	211.3	29.1	211.8	30.7
		$\lambda$	0.001	0.0005	0.01	0.0005
		$\lambda_{TV}$	0.0001	0.0001	0.0001	0.0001

TABLE III

THE REGULARIZATION PARAMETERS AND THE RUNNING TIME OF THE DIFFERENT UNMIXING ALGORITHM FOR THE REAL DATA

Real Data		SUnSAL-TV	SUnTV-sGSADMM	CLSUnSAL-TV	CLSUnTV-sGSADMM
	Parameters	$\lambda = 0.001, \lambda_{TV}=0.0001$	$\lambda = 0.001, \lambda_{TV}=0.0001$	$\lambda = 0.001, \lambda_{TV}=0.0001$	$\lambda = 0.001, \lambda_{TV}=0.0001$
	time(s)	2745.5	254.9	2823.8	252.4

7 and Fig. 8 were obtained using the optimal parameters  $\lambda$  and  $\lambda_{TV}$  which are given in Table I and Table II. We can see from Fig. 6, Fig. 7 and Fig. 8 that the unmixing performance of the dual sGS-ADMM is as good as that of the pADMM.

By and large, the priority of the dual sGS-ADMM lies in the less computing time and the relatively higher SRE value. The reason is that for the pADMM, it introduces several variables which directly lead to smaller iteration steps, while the dual sGS-ADMM takes relatively larger steps. And very small steps may not achieve an ideal SRE value which the model problem

can supply in a reasonable amount of time. In other words, even for the same problem, the algorithm we choose is also important.

## VII. NUMERICAL RESULTS WITH THE REAL DATA

The real hyperspectral remote sensing data is from a very famous Airborne Visible Infrared Imaging Spectrometer (AVIRIS) Cuprite data set.<sup>5</sup> The data used in our experiments

<sup>5</sup> Available online: <http://aviris.jpl.nasa.gov/html/aviris.freedata.html>.

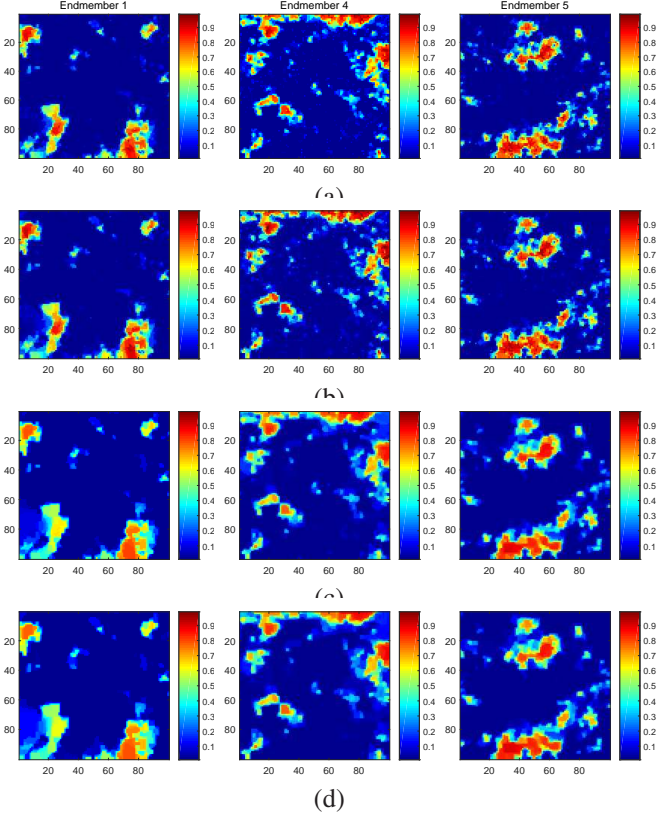


Fig. 8. The estimated abundances obtained by the different unmixing algorithms for endmember 1, endmember 4, and endmember 5 in the DC 3 with SNR = 20 dB (white noise). From top to bottom: (a) SUnSAL-TV, (b) SUnTV-sGSADMM, (c) CLSUnSAL-TV, (d) CLSUnTV-sGSADMM.

corresponds to a  $250 \times 191$ -pixel subset of the sector labeled as f970619t01p02\_r02\_sc03.a.rfi in the online data. The scene comprises 224 spectral bands between 0.4 and  $2.5 \mu\text{m}$ , with nominal spectral resolution of 10 nm. Prior to the analysis, bands 1-2, 105-115, 150-170, 223-224 were cut off because of water absorption and low SNR in those bands, leaving a total of 188 spectral bands. The spectral library used here is to select 498 spectra from the USGS spectral library and remove the corresponding bands. The regularization parameters and the computing time of the different unmixing algorithms for the real data are given in Table III. As one can see from Table III, our proposed algorithm is about 10 times faster than the pADMM. We can just make a visual comparison on the abundances map of the minerals since the true abundances of the real data are unknown. Fig. 9 shows the estimated abundances obtained by the different unmixing algorithms for the mineral: alunite, buddingtonite, chalcedony. From Fig. 9, it can be observed that the effects by the SUnTV-sGSADMM and the CLSUnTV-sGSADMM are as good as those by the SUnSAL-TV and the CLSUnSAL-TV.

## VIII. CONCLUSION

In this paper, we developed an efficient and convergent dual sGS-ADMM for the hyperspectral sparse unmixing with a TV regularization term. As shown in the numerical experiments, this approach can obviously improve the efficiency of the

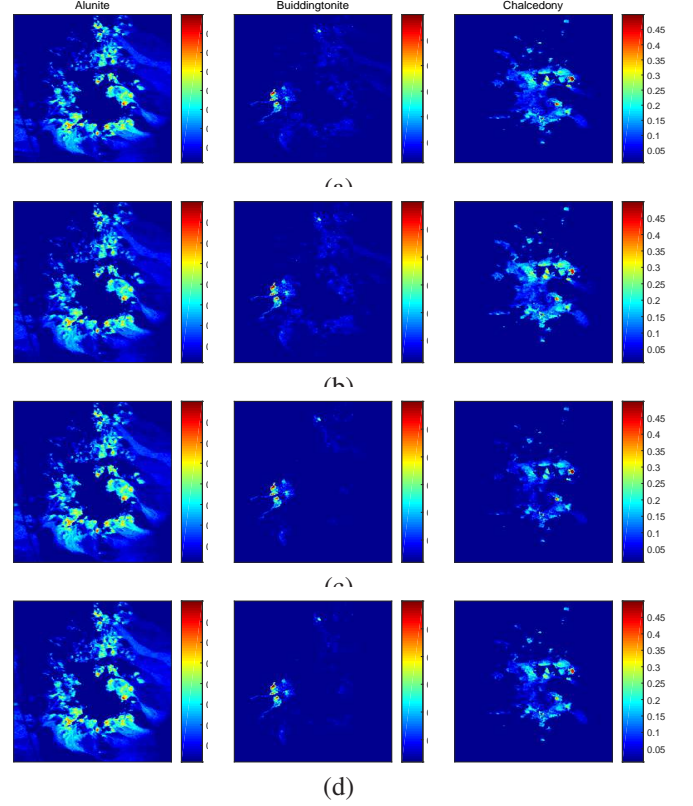


Fig. 9. The estimated abundances obtained by the different unmixing algorithms for the mineral: alunite, buddingtonite, chalcedony. From top to bottom: (a) SUnSAL-TV, (b) SUnTV-sGSADMM, (c) CLSUnSAL-TV, (d) CLSUnTV-sGSADMM.

unmixing compared with the state-of-the-art algorithm. More importantly, we can obtain relatively higher SREs for different problems.

## APPENDIX A PROOF OF THEOREM 1

*Proof 1:* We note that Algorithm 1 is actually the SPADMM. According to [28, Theorem B.1], we only need to prove the following condition holds.

$$\Sigma_f + \sigma \mathbf{F}^T \mathbf{F} \succ 0, \quad (15)$$

where

$$\Sigma_f := \begin{pmatrix} \mathbf{0}_{m \times m} & \mathbf{0}_{m \times L} & \mathbf{0}_{m \times m} & \mathbf{0}_{m \times m} \\ \mathbf{0}_{L \times m} & \mathbf{I}_{L \times L} & \mathbf{0}_{L \times m} & \mathbf{0}_{L \times m} \\ \mathbf{0}_{m \times m} & \mathbf{0}_{m \times L} & \mathbf{0}_{m \times m} & \mathbf{0}_{m \times m} \\ \mathbf{0}_{m \times m} & \mathbf{0}_{m \times L} & \mathbf{0}_{m \times m} & \mathbf{0}_{m \times m} \end{pmatrix}.$$

By simple calculations, we know that the condition (15) is equivalent to that

$$\begin{pmatrix} \mathbf{A}^T \mathbf{A} + 3\mathbf{I}_{m \times m} & -\mathbf{A}^T & -\mathbf{I}_{m \times m} & -\mathbf{I}_{m \times m} \\ -\mathbf{A} & \frac{\sigma+1}{\sigma} \mathbf{I}_{L \times L} & \mathbf{0}_{L \times m} & \mathbf{0}_{L \times m} \\ -\mathbf{I}_{m \times m} & \mathbf{0}_{m \times L} & \mathbf{I}_{m \times m} & \mathbf{0}_{m \times m} \\ -\mathbf{I}_{m \times m} & \mathbf{0}_{m \times L} & \mathbf{0}_{m \times m} & \mathcal{H}^T \mathcal{H} + \mathbf{I}_{m \times m} \end{pmatrix}$$

is positive definite. From the Schur complement condition [33], we only need to require that  $\mathbf{S}$  is positive definite.

## APPENDIX B

### PROOF OF THEOREM 2

*Proof 2:* We note that the dual sGS-ADMM is essentially a special case of the SPADMM. According to [28, Theorem B.1], in order to prove the convergence, we only need to prove the following condition holds.

$$\Sigma_\psi + \sigma \mathcal{A}^* \mathcal{A} + \mathcal{T} \succ 0, \quad (16)$$

where

$$\begin{aligned} \Sigma_\psi &:= \begin{pmatrix} \mathbf{0}_{m \times m} & \mathbf{0}_{m \times L} \\ \mathbf{0}_{L \times m} & \mathbf{I}_{L \times L} \end{pmatrix}, \\ \mathcal{T} &:= \mathcal{U} \mathcal{D}^{-1} \mathcal{U}^T = \begin{pmatrix} \mathbf{0}_{m \times m} & \sigma \mathbf{A}^T \\ \mathbf{0}_{L \times m} & \mathbf{0}_{L \times L} \end{pmatrix} \\ &\quad \begin{pmatrix} \sigma^{-1} \mathbf{I}_{m \times m} & \mathbf{0}_{m \times L} \\ \mathbf{0}_{L \times m} & (\mathbf{I}_{L \times L} + \sigma \mathbf{A} \mathbf{A}^T)^{-1} \end{pmatrix} \begin{pmatrix} \mathbf{0}_{m \times m} & \mathbf{0}_{m \times L} \\ \sigma \mathbf{A} & \mathbf{0}_{L \times L} \end{pmatrix} \\ &= \begin{pmatrix} \sigma \mathbf{A}^T (\sigma^{-1} \mathbf{I}_{L \times L} + \mathbf{A} \mathbf{A}^T)^{-1} \mathbf{A} & \mathbf{0}_{m \times L} \\ \mathbf{0}_{L \times m} & \mathbf{0}_{L \times L} \end{pmatrix}. \end{aligned}$$

By simple calculations, we know that (16) is equivalent to that

$$\begin{pmatrix} \mathbf{I} + \mathbf{A}^T (\sigma^{-1} \mathbf{I}_{L \times L} + \mathbf{A} \mathbf{A}^T)^{-1} \mathbf{A} & \mathbf{A}^T \\ \mathbf{A} & \sigma^{-1} \mathbf{I}_{L \times L} + \mathbf{A} \mathbf{A}^T \end{pmatrix}$$

is positive definite. From the Schur complement condition [33], we only need to require that  $\mathbf{T}$  is positive definite.

## ACKNOWLEDGEMENTS

We would like to thank Professor Xile Zhao at School of Mathematics, University of Electronic Science and Technology of China for his useful comments and suggestions. We also thank Professor Hengchao Li at School of Information Science and Technology, Southwest Jiaotong University for fruitful discussions.

## REFERENCES

- [1] J. M. Bioucas-Dias, A. Plaza, N. Dobigeon, M. Parente, Q. Du, P. Gader, and J. Chanussot, "Hyperspectral unmixing overview: Geometrical, statistical, and sparse regression-based approaches," *IEEE J. Sel. Topics Appl. Earth Observ. Remote Sens.*, vol. 5, no. 2, pp. 354-379, Apr. 2012.
- [2] J. P. Nascimento and J. M. Bioucas-Dias, "Vertex component analysis: A fast algorithm to unmix hyperspectral data," *IEEE Trans. Geosci. Remote Sens.*, vol. 43, no. 4, pp. 898-910, Apr. 2005.
- [3] J. W. Boardman, F. A. Kruse, and R. O. Green, "Mapping target signatures via partial unmixing of AVIRIS data," in *Proc. JPL Airborne Earth Sci. Workshop.*, 1995, pp. 23-26.
- [4] C.-I. Chang, C.-C. Wu, W. Liu, and Y.-C. Ouyang, "A new growing method for simplex-based endmember extraction algorithm," *IEEE Trans. Geosci. Remote Sens.*, vol. 44, no. 10, pp. 2804-2819, Oct. 2006.
- [5] T.-H. Chan, C.-Y. Chi, Y.-M. Huang, and W.-K. Ma, "Convex analysis based minimum-volume enclosing simplex algorithm for hyperspectral unmixing," *IEEE Trans. Signal Process.*, vol. 57, no. 11, pp. 4418-4432, Nov. 2009.
- [6] M. Berman, H. Kiiveri, R. Lagerstrom, A. Ernst, R. Dunne, and J. F. Huntington, "ICE: A statistical approach to identifying endmembers in hyperspectral images," *IEEE Trans. Geosci. Remote Sens.*, vol. 42, no. 10, pp. 2085-2095, Oct. 2004.
- [7] L. Miao and H. Qi, "Endmember extraction from highly mixed data using minimum volume constrained nonnegative matrix factorization," *IEEE Trans. Geosci. Remote Sens.*, vol. 45, no. 3, pp. 765-777, Mar. 2007.
- [8] N. Dobigeon, S. Moussaoui, M. Coulon, J.-Y. Tourneret, and A. O. Hero, "Joint Bayesian endmember extraction and linear unmixing for hyperspectral imagery," *IEEE Trans. Signal Process.*, vol. 57, no. 11, pp. 4355-4368, Nov. 2009.

- [9] E. J. Candès and T. Tao, "Decoding by linear programming," *IEEE Trans. Inf. Theory.*, vol. 51, no. 12, pp. 4203-4215, Dec. 2005.
- [10] E. J. Candès, J. Romberg, and T. Tao, "Stable signal recovery from incomplete and inaccurate measurements," *Commun. Pure Appl. Math.*, vol. 59, no. 8, pp. 1207-1223, Aug. 2006.
- [11] A. M. Bruckstein, D. L. Donoho, and M. Elad, "From sparse solutions of systems of equations to sparse modeling of signals and images," *SIAM Rev.*, vol. 51, no. 1, pp. 34-81, Feb. 2009.
- [12] M.-D. Iordache, J. M. Bioucas-Dias, A. Plaza, and B. Somers, "MUSIC-CSR: Hyperspectral unmixing via multiple signal classification and collaborative sparse regression," *IEEE Trans. Geosci. Remote Sens.*, vol. 52, no. 7, pp. 4364-4382, Jul. 2014.
- [13] E. J. Candès, J. Romberg, and T. Tao, "Robust uncertainty principles: Exact signal reconstruction from highly incomplete frequency information," *IEEE Trans. Inf. Theory.*, vol. 52, no. 2, pp. 489-509, Feb. 2006.
- [14] M.-D. Iordache, J. M. Bioucas-Dias, and A. Plaza, "Sparse unmixing of hyperspectral data," *IEEE Trans. Geosci. Remote Sens.*, vol. 49, no. 6, pp. 2014-2039, Jun. 2011.
- [15] M.-D. Iordache, J. M. Bioucas-Dias, and A. Plaza, "Total variation spatial regularization for sparse hyperspectral unmixing," *IEEE Trans. Geosci. Remote Sens.*, vol. 50, no. 11, pp. 4484-4502, Nov. 2012.
- [16] A. Beck and M. Teboulle, "Fast gradient-based algorithms for constrained total variation image denoising and deblurring problems," *IEEE Trans. Image Process.*, vol. 18, no. 11, pp. 2419-2434, Nov. 2009.
- [17] M. V. Afonso, J. M. Bioucas-Dias, and M. A. T. Figueiredo, "Fast image recovery using variable splitting and constrained optimization," *IEEE Trans. Image Process.*, vol. 19, no. 9, pp. 2345-2356, Sep. 2010.
- [18] M. V. Afonso, J. M. Bioucas-Dias, and M. A. T. Figueiredo, "An augmented Lagrangian approach to the constrained optimization formulation of imaging inverse problems," *IEEE Trans. Image Process.*, vol. 20, no. 3, pp. 681-695, Mar. 2011.
- [19] H. E. Güven, A. Güngör, and M. Çetin, "An augmented Lagrangian method for complex-valued compressed SAR imaging," *IEEE Trans. Comput. Imag.*, vol. 2, no. 3, pp. 235-250, Sep. 2016.
- [20] S. Zhang, J. Li, K. Liu, and A. Plaza, "Hyperspectral unmixing based on local collaborative sparse regression," *IEEE Geosci. Remote Sens. Lett.*, vol. 13, no. 5, pp. 631-635, May. 2016.
- [21] L. Zhang, W. Wei, Y. Zhang, H. Yan, F. Li, and C. Tian, "Locally similar sparsity-based hyperspectral compressive sensing using unmixing," *IEEE Trans. Comput. Imag.*, vol. 2, no. 2, pp. 86-100, Jun. 2016.
- [22] M.-D. Iordache, J. M. Bioucas-Dias, and A. Plaza, "Collaborative sparse regression for hyperspectral unmixing," *IEEE Trans. Geosci. Remote Sens.*, vol. 52, no. 1, pp. 341-354, Jan. 2014.
- [23] Y.-J. Chen, W.-D. Ge, and L. Sun, "A novel linear hyperspectral unmixing method based on collaborative sparsity and total variation," *Acta Auto. Sinica.*, vol. 44, no. 1, pp. 116-128, Jan. 2018.
- [24] R. Glowinski and A. Marroco, "Sur l'approximation, par éléments finis d'ordre un, et la résolution, par pénalisation-dualité d'une classe de problèmes de Dirichlet non linéaires," *Revue Française d'Automatique, Informatique et Recherche Opérationnelle*, vol. 2, no. R-2, pp. 41-76, Jan. 1975.
- [25] D. Gabay and B. Mercier, "A dual algorithm for the solution of nonlinear variational problems via finite element approximation," *Comput. Math. Appl.*, vol. 2, no. 1, pp. 17-40, Dec. 1976.
- [26] J. Eckstein and W. Yao, "Understanding the convergence of the alternating direction method of multipliers: Theoretical and computational perspectives," *Pac. J. Optim.*, vol. 11, no. 4, pp. 619-644, Oct. 2015.
- [27] R. Glowinski, "On alternating direction methods of multipliers: A historical perspective," in *W. Fitzgibbon, Y. A. Kuznetsov, P. Neittaanmaki and O. Pironneau (eds.), Modeling, Simulation and Optimization for Science and Technology.*, Springer, Netherlands, pp. 59-82, 2014.
- [28] M. Fazel, T. K. Pong, D. Sun, and P. Tseng, "Hankel matrix rank minimization with applications to system identification and realization," *SIAM J. Matrix Anal. Appl.*, vol. 34, no. 3, pp. 946-977, Jul. 2013.
- [29] D. Han, D. Sun, and L. Zhang, "Linear rate convergence of the alternating direction method of multipliers for convex composite programming," arXiv:1508.02134, Aug. 2015.
- [30] C. Chen, B. He, Y. Ye, and X. Yuan, "The direct extension of ADMM for multi-block convex minimization problems is not necessarily convergent," *Math. Program.*, vol. 155, no. 1-2, pp. 57-79, Jan. 2016.
- [31] X. Li, D. Sun, and K.-C. Toh, "A block symmetric Gauss-Seidel decomposition theorem for convex composite quadratic programming and its applications," *Math. Program.*, pp. 1-24, Feb. 2018.
- [32] R. T. Rockafellar, "Convex Analysis," Princeton, NJ, USA: Princeton Univ. Press, 1970.
- [33] R. A. Horn and C. R. Johnson, "Matrix Analysis," Cambridge, UK: Cambridge Univ. Press, 1985.

- [34] J. Sun, "On monotropic piecewise quadratic programming," Ph.D. dissertation, Univ. Washington, Seattel, USA, 1986.
- [35] S. M. Robinson, "Some continuity properties of polyhedral multifunctions," *Math. Program. Study*, vol. 14, pp. 206-214, Oct. 1981.
- [36] A. Dontchev and R. T. Rockafellar, "Implicit Function and Solution Mappings," New York, NY, USA: Springer, 2009.
- [37] R. T. Rockafellar and R. J. -B. Wets, "Variational Analysis," New York, NY, USA: Springer, 1998.
- [38] R. Wang, H.-C. Li, W. Liao, X. Huang, and W. Philips, "Centralized collaborative sparse unmixing for hyperspectral images," *IEEE J. Sel. Topics Appl. Earth Observ. Remote Sens.*, vol. 10, no. 5, pp. 1949-1962, May. 2017.
- [39] L. Condat, "A direct algorithm for 1-D total variation denoising," *IEEE Signal Process. Lett.*, vol. 20, no. 11, pp. 1054-1057, Nov. 2013.
- [40] J. Friedman, T. Hastie, H. Höfling, and R. Tibshirani, "Pathwise coordinate optimization," *Ann. Appl. Stat.*, vol. 1, no. 2, pp. 302-332, Aug. 2007.
- [41] W.-K. Ma, J. M. Bioucas-Dias, T.-H. Chan, N. Gillis, P. Gader, A. Plaza, A. Ambikapathi, and Chong.-Y. Chi, "A signal processing perspective on hyperspectral unmixing: Insights from remote sensing," *IEEE Signal Process. Magazine.*, vol. 31, no. 1, pp. 67-81, Jan. 2014.
- [42] B. Kozintsev, "Computations with Gaussian random fields," Ph.D. dissertation, Univ. Maryland, College Park, MD, USA, 1999.
- [43] Y. Yu, "On decomposing the proximal map," *Adv. Neural Inform. Process. Syst.* vol. 1, pp. 91-99, Dec. 2013.